THIN-BEDDED TURBIDITES AND CHANNEL SANDS: THE CONNECTIVITY BRIDGE

BAYONLE ABIOLA OMONIYI

Submitted for the degree of Doctor of Philosophy

Heriot-Watt University
Institute of Petroleum Engineering

September 2017

ABSTRACT

Turbidite deposits are a common facies in many deepwater systems, and within these facies, thin-bedded turbidites (TBTs) and very thin-bedded turbidites (VTBTs) are most abundant, but their potential for exploration and production has been largely underdeveloped. This study seeks to develop a quantitative approach for characterisation of TBTs and VTBTs, using their sedimentary attributes from ancient and subsurface systems, to assess the impact of multi-scale sedimentary heterogeneity on the connectivity between TBT/VTBT intervals and other turbidite facies within selected deepwater systems. It further seeks to provide valuable insights into the hidden reservoir potential of TBT/VTBT facies, with a view to assessing their capability to enhance or reduce the impact of net-to-gross-associated uncertainty on connectivity between these facies and associated primary reservoir facies (channel sands).

Analysis of 1,107 ft (337.4 m) of cores from the North Brae Field enabled identification of the sedimentary attributes of TBT/VTBT facies and their combination into attribute indices. These indices are *facies* Net-to-Gross Index (NGI), Sand Connectivity Index (SCI), Facies Ratio Index (FRI), and Sediment Textural Index (STI). From these indices, NGI and SCI form the central focus of this study. The interpreted sedimentary logs together with the insights gained from an additional 16,275 ft (4, 961 m) of cores logged from Pierce, Starling, and Fram Fields, enhanced the appreciation of multi-scale lateral and vertical variabilities of their facies attributes. The detailed study undertaken on an 892 ft (272 m)-long interval in the Zumaia section, serves to provide the input data for the high-resolution modelling and flow simulation studies conducted to better understand the importance of bed-scale sedimentary heterogeneities on fluid flow in a typical basin-plain setting. In addition, the resultant multi-resolution models reflect significant variations in the distribution of key parameters that affect flow performance within the types of connectivity bridge (defined in this thesis as the connectivity between primary and secondary reservoir facies) considered.

The results of this study demonstrate that attribute indices can be applied to characterise different deepwater architectural elements, and also serve as quantitative input parameters for conditioning reservoir models and ground-truthing flow simulation. This application can be extended to all turbidite types. Furthermore, the results indicate the importance of siting injector wells strategically to improve oil sweep, and minimise the risk of high water cut, whilst optimising oil recovery. The findings establish the effect of bed-scale sedimentary heterogeneity, particularly bed stacking pattern, net-to-gross

distribution, and lateral variation in bed thickness, on connectivity, which in turn has profound implications on the producibility of deepwater turbidite reservoirs, and can therefore have a significant effect on reserve estimation and overall project value. On the basis of the Continuity-Connectivity Scheme, developed from isolating individual continuity-connectivity relationships in the various scenarios considered, TBT-associated deepwater turbidite systems can be classified into six broad categories, namely: (1) low continuity and high connectivity systems (single-storey channel); (2) low-to-intermediate continuity and intermediate connectivity systems (laterally-stacked channel-levee); (3) intermediate continuity and low connectivity systems (distal basin plain); (4) intermediate-to-high continuity and intermediate-to-high connectivity systems (vertically-stacked channel-levee); (5) high continuity and intermediate connectivity systems (proximal basin plain); and (6) high continuity and high connectivity systems (channel-splay lobe).

Following the results of this study, deepwater turbidite reservoirs that are characterised by an effective oil displacement, efficient areal sweep, and lowest risk to early water breakthrough offer the best potential, occasioned by a favourable connectivity threshold, for economic recovery of bypassed pay in hydrocarbon-producing turbidite fields.

DEDICATION

This PhD thesis is dedicated to the Creator of Heaven and Earth, and to my family.

ACKNOWLEDGEMENTS

I express my sterling gratitude to the God of my fathers, the Creator of Heaven and Earth, my Saviour and Strength, my Refuge and Fortress, my Provider and Healer, and the Keeper of my destiny.

I am heartily grateful to the Federal Government of Nigeria for the Tertiary Education Trust Fund Scholarship that made it possible for me to undertake PhD research in the United Kingdom. I am equally grateful to Heriot-Watt University for considering me for a James Watt Scholarship, without which it would be practically impossible to complete this programme.

I owe an enormous debt of gratitude to my principal supervisor, Professor Dorrik A. V. Stow, for his trust and genuine kindness to me throughout the programme. His unfailing support and encouragements towards conference presentations beats my imagination, and his constructive criticisms provided me with the drive to achieve success in the programme. I would also like to thank my supporting supervisor, Dr Andy Gardiner, for his support and helpful criticisms, particularly during the early stages of the research. Professor Eric MacKay, Professor Sebastian Geiger, Dr Helen Lever, Dr Helen Lewis, and Dr Gillian Pickup are equally appreciated. I am grateful to Mrs Jane Wells, Mrs Sally Hamilton, Mrs Jill Prior, Mrs Angela Nelson, Mrs Pamela Pendreigh, Mrs Debbie Ross, and the entire staff at the IPE Postgraduate Research Student Support for their advice. Dr Jim Buckman, Dr Eltazy Khalid, Mr Dominic Tatum, Mr Alan Brown, and Mr Christopher Leonard are equally thanked for their assistance.

I acknowledge the substantial support of Dr Colin Turner to the TBT research, through the cores supplied and scheduled visits. Professor Bryan Cronin is equally appreciated for insightful discussions on the depositional architecture of the North Brae Field. Dr Efthymios Tripsanas is greatly appreciated for invitations to make research presentations at Shell, Aberdeen, and access to cores from Pierce, Starling, and Fram Fields, in addition to his generous support. I am profoundly grateful to Mrs Claire Ashford for her assistance in proof-reading the thesis draft. All my colleagues are appreciated, particularly Mr Urval Patel, Dr Rachel Brackenridge, Mrs Mina Esentia, and Ms Anastasia Polymeni for making me feel welcome at the start of the programme.

I express my profound gratitude to my lovely wife, Barrister (Mrs) Jumoke Omoniyi, for her sacrifice, unwavering support and unconditional love. My children, Oluwaseyi, Oluwatosin, and Oluwabukunmi are greatly appreciated for their love, prayers, and cooperation. My lovely mother, Mrs Eunice Omoniyi, is warmly appreciated for her prayers and understanding.

DECLARATION STATEMENT

(Research Thesis Submission Form should be placed here)

TABLE OF CONTENTS

Page

PART 1: INTRODUCTION TO THESIS AND LITERATURE REVIEW

PART 2: DATABASE AND METHODS

PART 3: RESULTS

LIST OF TABLES

LIST OF FIGURES

ABBREVIATIONS

Psi	Pounds per square inch
psi/ft	Pounds per square inch per foot
Kh	Horizontal permeability
Kv	Vertical permeability
k_n	Permeability to nitrogen
OIIP	Oil initially in place
OIP	Oil in place
GIIP	Gas initially in place
GIP	Gas in place
WIIP	Water initially in place
WIP	Water in place
MMBBL	Million barrels
SCF	Standard cubic feet
MMSCF	Million standard cubic feet
BCF	Billion cubic feet
BBOE	Billion barrels oil equivalent recoverable
BOPD	Barrels of oil per day
BWPD	Barrels of water per day
BBL	Barrel(s)
BBL/D	Barrels per day
MMSCF/D	Million standard cubic feet per day
in	inches
ft	Feet
cm	centimetre
m	metre
m/s	metre per second
cm/s	centimetre per second
m^3	cubic metre
g/m^3	gram per cubic metre
kg/m^3	kilogram per cubic metre
m^3/d	cubic metre per day
y	year
m/ky	metre/thousand years

HDTs	high-density turbidity currents
LDTs	low-density turbidity currents
mg/l	milligram per litre
mm	millimetre
mD	milliDarcy
VTBT	Very thin-bedded turbidites (turbidite beds with 1-3 cm thick sand/silt unit)
TBT	Thin-bedded turbidites (turbidite beds with 3-10 cm thick sand/silt unit)
NGI	Net-to-gross index
VCI	Vertical connectivity index
LCI	Lateral connectivity index
SCI	Sand connectivity index
FRI	Facies ratio index
STI	Sediment textural index
~	Approximately
TVDSS	True vertical depth subsurface
MD	Measured depth

LIST OF PUBLICATIONS

1. **Thin-bedded Turbidites: Overview and Petroleum Perspective.**
   Dorrik A. V. Stow and Bayonle A. Omoniyi
   (AAPG Memoir 115; accepted for publication)

2. **Characterisation of Thin-bedded Turbidites in the North Brae Field, South Viking Graben, North Sea.**
   Bayonle A. Omoniyi, Dorrik A. V. Stow and A. R. Gardiner
   (AAPG Memoir 115; accepted for publication)

PART 1

INTRODUCTION TO THESIS AND LITERATURE REVIEW

Chapter 1

Introduction to thesis

Photo by Bayonle Omoniyi

Deepwater turbidite succession (near Monk's Cave)
Silurian Mynydd Bach Formation
Aberystwyth Grits Group
Ceredigion (Mid Wales), UK

This chapter provides a general introduction to this thesis and how it is organised.

References have been collated at the end of the thesis.

1.1 THESIS OVERVIEW

Thin-bedded turbidites are arguably the dominant facies in deepwater systems, occurring throughout the spectrum of architectural elements in deepwater environments (Stow et al., 1996; Stow, 2000; Stow & Mayall, 2000). They present underestimated potential within deepwater turbidite exploration and production (Weimer et al., 2000; Shanmugam, 2006). They have huge significance as both principal and marginal reservoirs, and for optimising production from existing reservoirs. They have further significance as deepwater source rocks, potential unconventional reservoirs and, in the case of mud-rich (thin and thick-bedded) turbidites, even as reservoir seals (Stow and Omoniyi, in press).

A large proportion of the world's major hydrocarbon reservoirs occur in deep-water turbidite systems (Pettingill, 1998; Stow, 2000; Stow & Mayall, 2000; Khain & Polyakova, 2004; Gluyas & Garrett, 2005; Hurst et al., 2005). Exploration in deep water is increasingly active, with more than 50% of new discoveries in the past 10 years coming from deepwater plays. In the enterprise of growing reserves and optimising field value in producing and marginal turbidite fields, the significance of thin-bedded turbidites (TBT – 3-10 cm thick sand/silt unit) and very thin-bedded turbidites (VTBT – 1-3 cm thick sand/silt unit) cannot be overemphasised.

TBTs occur as separate facies and may be sandwiched between intervals of thick (30-100 cm) and very thick-bedded turbidites (over 100 cm). Although some TBT facies have poor reservoir quality, others have good reservoir quality to significantly enhance hydrocarbon reserves in fields producing from deepwater sandstones (Shepherd, 1991; Clemenceau, 1995; Lerch et al., 1996; Clemenceau et al., 2000; Browne & Slatt, 2002). In the Paleocene Forties Field, for example, over 100 pay zones that had been bypassed during the initial recovery phase (Hillier et al., 1978), were targeted for infill drilling in 2003, resulting in a mature stage peak production of 50,000-60,000 BOPD (Rose & Pyle, 2015). In another instance, they form the oil-bearing zone within the Early Cretaceous Scapa Sandstone Member in the Scapa Field (McGann et al., 1991), and in the Magnus Field, they contribute to reserves, enabling extension of field life (Shepherd, 1991; MacGregor et al., 2005). Despite this potential, low net-to-gross, poorly connected TBT/VTBT units are capable of forming stratigraphic compartments that effectively trap oil within turbidite reservoirs. This trapped oil, where it is economically justified to recover like in the Forties Field, can be pivotal in delaying production decline and achieving field value optimization.

For enhanced sweep during waterflood production, recovery of bypassed oil can only be achieved when key properties that control fluid flow in the stratigraphic compartments are adequately understood. These properties include lateral changes in bed thickness, internal facies geometry and distribution, facies continuity and connectivity within and in association with primary reservoir sands, permeability contrast between primary reservoir facies and TBT/VTBT facies, internal architecture, and scale of heterogeneity.

This thesis, therefore, seeks to contribute to the knowledge base of thinly bedded turbidite facies, in particular, and turbidite reservoirs, in general, through a set of objectives that are outlined in section 1.2. It applies the multidisciplinary skills of sedimentology, petroleum geoscience (development and production), reservoir engineering, and reservoir flow simulation.

1.2 RESEARCH OBJECTIVES

i. Appraisal of TBT/VTBT depositional processes and resultant facies and sequences within the range of deepwater architectural elements with a view to improving the understanding of their geological (specifically, sedimentary) attributes.

ii. Development of a novel quantitative approach for characterisation of TBT/VTBT facies, in order to characterise the various sedimentary attributes of TBT successions in a way that can be easily quantified for application to reservoir models. This approach will be used as parametric quantities for quantifying the core attributes such as net-to-gross and facies connectivity.

iii. Application of the quantitative approach as a tool to predict lateral and vertical connectivities within individual TBT/VTBT packages and in associated turbidite reservoir intervals. Where TBT/VTBT sequences form secondary reservoir intervals, the approach is to be applied to a variety of possible architectural elements with a view to understanding the impact of their sedimentary heterogeneity and resultant connectivity on the primary reservoir facies, notably channel and lobe sands. In particular, the research will seek to address the impact of variable sedimentary heterogeneity across the ‘connectivity bridge’

(defined here as the connectivity between primary and secondary reservoir facies) on fluid flow and oil recovery.

iv. Evaluate small-scale sedimentary heterogeneity in TBT/VTBT attributes and its impact on oil recovery from related reservoir architecture. Quantify the associated uncertainties to oil recovery from turbidite reservoirs with similar architecture.

v. Assess the critical risks posed by TBT/VTBT facies to oil recovery from the primary reservoir facies, and quantify associated uncertainties to oil initially in place, oil production rate, oil recovery efficiency, water cut, cumulative oil production, and long-term forecast of oil production rate decline.

vi. Develop a series of waterflood simulations to capture the connectivity between primary reservoir sands, within channel and lobe geometries with a view to analysing vertical and horizontal flow behaviour in such reservoirs.

vii. Quantify the impact of uncertainty in net-to-gross on connectivity of TBT/VTBT and associated channel sands with a view to providing an insight into the relationship between net-to-gross and connectivity in conceptualised channelised settings.

1.3 THESIS RATIONALE

TBT/VTBT facies are characterised by a high degree in heterogeneity, varying in facies and facies associations, sand and shale geometry, sediment fabric and microfabric, sand and shale geometry, sand and shale dimensions, sediment texture, sand connectivity, sandstone-mudstone ratio, small-scale sedimentary structures and small-scale vertical sequences of bed thickness (Figure 1.1). The resultant anisotropic properties have considerable impact on fluid flow within TBT/VTBT reservoir intervals. They are also significant for fluid flow across the ‘connectivity bridge’ between TBT/VTBT zones and thicker-bedded reservoir zones of channels, lobes or other associated reservoir facies.

This thesis sets out to provide valuable insights into the connectivity of TBT/VTBT within their respective intervals and between associated channel sands or

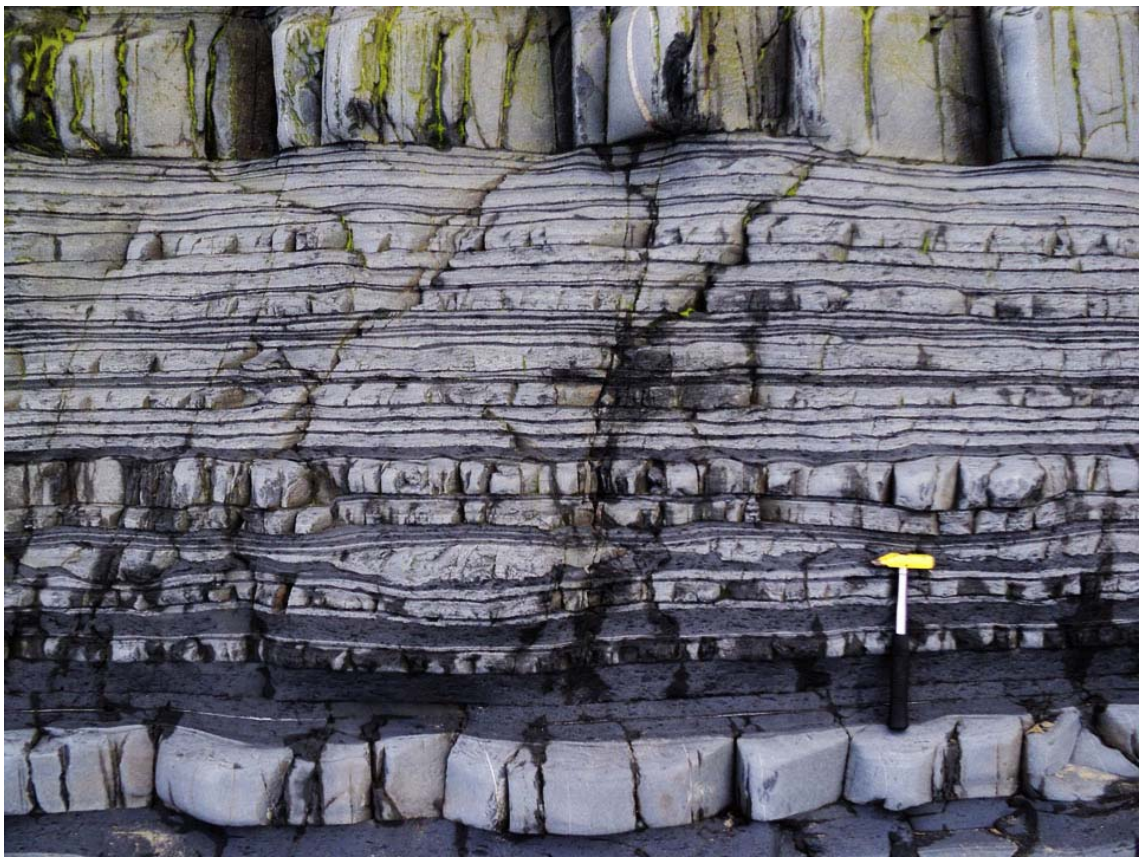

Figure 1.1. Selected photograph of TBT/VTBT facies from a turbidite outcrop in New Quay, Silurian Mynydd Bach Formation, Aberystwyth Grits Group, Mid Wales. The TBT/VTBT facies are sandwiched between adjacent thick-bedded turbidites. The TBT/VTBT facies considerably vary in their bed continuity, sandstone-mudstone ratio, sand and shale dimensions, sediment fabric and microfabric, sand and shale geometry, sediment texture, sand connectivity, small-scale sedimentary structures, and small-scale vertical sequences of bed thickness. In terms of fluid flow, the scale of the variation in their properties influence their dynamic characteristics, either as baffles to flow, or as barriers to communication of principal reservoir sand bodies.

primary reservoir facies at inter-well scale. This will help to inform prediction of connectivity within and across turbidite reservoir architecture and at bed scale for assessment of the impacts of bed-scale heterogeneity on connectivity within TBT/VTBT successions and with associated thicker-bedded reservoir facies.

It is hoped that the results presented in this thesis will provide a better understanding of connectivity between TBT/VTBT facies association packages and associated thicker-bedded turbidite reservoir facies, to enable a robust quantitative characterisation of their attributes and flow properties, in addition to prediction of production performance where they are an important component of turbidite reservoirs. The insights gained will help to unlock the reservoir potential of TBT/VTBT where they have been bypassed/unswept by the initial recovery phase.

1.4 THESIS ORGANISATION

This thesis comprises four parts and a total of nine chapters (Table 1.1). Part 1 consists of Chapters 1 and 2. Chapter 1 introduces this thesis. Chapter 2 provides a state-of-the-art synthesis of what we do know about TBT/VTBT systems based on detailed bibliographic research and fieldwork in Mid Wales (United Kingdom) and Basque Country (Spain), and what is largely unknown. It describes the standard models for TBT/VTBT facies and evaluates the concept of connectivity in the light of what has been done and why the novel quantitative approach developed in this thesis presents a better alternative for estimating connectivity in TBT/VTBT-associated deepwater turbidite reservoirs. The chapter addresses the first objective of the research. Understanding gained from outcrop studies covering Silurian turbidite successions in the Trefechan and Mynydd Formations in Mid Wales, and Eocene succession of the Itzurun Formation, exposed at Zumaia, was useful in preparing various sections in this chapter. In addition to the study of ancient systems in these locations, valuable insights gained from describing cores recovered from the North Brae, Pierce, Starling, and Fram Fields were useful in describing relevant sections in this chapter. These sections make up part of a joint publication with my principal supervisor, Professor Dorrik Stow, in AAPG Memoir 115 (Turner and Cronin, 2017 in press).

Part 2 has one chapter (Chapter 3) that aims to provide a brief discussion on database for the research and a range of methods used and developed in this research. In particular, this chapter explains the development of ‘attribute indices’ method (second

Table 1.1. Thesis Organisation

Thesis Part and Title	**Thesis Chapter**	**Chapter Title**
1. Introduction to Thesis and Literature Review	1	Introduction to Thesis
	2	Literature Review
2. Database and Methods	3	Database and Methods
3. Results	4	Characterisation of Thin-bedded Turbidites in the North Brae Field, South Viking Graben, North Sea
	5	The Impact on Oil Recovery of Turbidite Architecture across the Connectivity Bridge between Channel and Splay Lobe Facies: an Integrated Study
	6	The Impact of Bed-scale Sedimentary Heterogeneities on Oil Recovery in the Eocene Basin-plain Turbidite Successions of Zumaia Flysch, Northern Spain
	7	A Robust Quantitative Approach for assessing the Impact of Stratigraphic Architecture and Uncertainties in Net-to-gross on Connectivity and Reservoir Performance in a Channel to Overbank Setting of the North Brae Field, UKCS
4. Summary, Conclusions and Further Work	8	Summary
	9	Conclusions and Further Work

objective) as used throughout the thesis and sources from which the data used for calculating attribute indices were obtained. The chapter describes the procedure followed to conduct laboratory-based porosity and permeability measurements of selected plugs of TBT/VTBT facies cored from core recovered from well 16/07a-B27 in the North Brae Field. It also explains the basic principles and techniques that underlie reservoir modelling and flow simulation studies carried out to achieve objectives iii-vii. Techniques for uncertainty analysis and basic statistics adopted in this thesis are also introduced in this chapter.

Part 3 encompasses Chapters 4-7. In addition to Chapter 4, Chapters 5, 6 and 7 provide some interpretation and discussion of the principal results. Chapters 5 and 7 are tailored towards the third, fifth, sixth and seventh objectives, using North Brae Field data. Chapter 7, in particular, addresses TBT/VTBT facies and associated risks to oil recovery and also quantifies the impact of uncertainty in net-to-gross on connectivity in three different conceptualised channel settings. Chapter 6 focuses on the evaluation of small-scale sedimentary heterogeneity and its impact on oil recovery (fourth objective). The effect of continuous and discontinuous shales by acting as baffles and creating flow anisotropy through the creation of tortuous flow paths, is captured in this chapter. The chapter utilises outcrop data from the Eocene turbidite succession of Zumaia section in the Itzurun Formation (Basque Country, Spain).

Part 4 provides a brief synthesis, discussion of principal achievements and conclusions of the thesis. Chapter 8 provides a general discussion to bring together the various aspects of the thesis that have been discussed individually in each of the previous chapters and the main achievements. This is followed by a brief chapter on conclusions and further work (Chapter 9).

The thesis has been written mainly as a series of papers for publication. Selected sections in Chapters 2 and 8 were combined into a research article, which together with Chapter 4 have been accepted for publication in AAPG Memoir 115 (Turner and Cronin, 2017 in press). Chapters 5-8 are still being finalised for submission to different high-impact Journals. To avoid repetition, abstracts and introductory sections have been left out of affected chapters. All references have been collated at the end of the thesis. Some additional data and figures are provided in the appendices, together with a series of conference abstracts indicating where the results have been presented so far.

Chapter 2

Literature Review

Photo by Bayonle Omoniyi

A TBT/VTBT section at Clarach
Silurian Trefechan Formation
Aberystwyth Grits Group
Ceredigion (Mid Wales), UK

This chapter synthesises what we know about TBT/VTBT systems and what is by and large unknown. Part of this chapter (together with selected sections in Chapter 8) was accepted as a joint publication with my principal supervisor, Professor Dorrik Stow, in AAPG Memoir 115 (Turner and Cronin, 2017 in press). Abstract is left out to avoid repetition, and references have been collated at the end of the thesis.

2.1 INTRODUCTION

A significant proportion of the world's major hydrocarbon reservoirs are found in deepwater siliciclastic systems (Reading & Richards, 1994; Pettingill, 1998; Stow & Mayall, 2000; Pettingill, 2004; Weimer & Pettingill, 2007). In the last decade alone, 50% of new discoveries have been from deepwater plays (Dorrik Stow, personal communication, 2016). These deepwater plays occur throughout the world, including the Gulf of Mexico, offshore West Africa, East Africa, Brazil, Australia, India, Southeast Asia, and offshore Northwest Europe (Figure 2.1). The principal reservoir targets in these present-day deepwater regions are turbidites and associated deepwater facies. Turbidites also form some of the main reservoirs and dominant plays in sedimentary basins that were originally deposited in deepwater, but are now on land or under shallow shelf settings, including the East Siberian Basin in Russia, the Ordos and Bohai Basins in China, and the United Kingdom North Sea. In the United Kingdom and Norwegian sectors of the North Sea, over 95% of oil production and 40% of gas production in the last two decades are from the Palaeogene and Jurassic submarine-fan (turbidite) reservoirs (Glennie, 1984; Brooks & Glennie, 1985; Richards et al., 1998). The principal fields in the North Sea that are producing from turbidite reservoirs are shown in Figure 2.2. A large proportion of these fields are mature fields that have within their reservoir intervals, thinly-bedded pay sections that have potential for growing reserves and slowing down production decline.

Indeed, most turbidite reservoirs comprise both thick (0.3-1.0 m) and very thick (over 1.0 m)-bedded turbidites in addition to thin-bedded turbidite (0.03-0.10 m; TBT) and very thin-bedded turbidites (<0.03 m; VTBT). These latter terms are often used loosely within the industry to mean 'beds below the resolution of conventional logging tools' but without a strict definition of bed thickness. The terms also generally refer to the sand portion of a turbidite bed. TBTs and VTBTs are arguably the dominant facies in deepwater systems, accumulating throughout a wide range of deepwater architectural elements, within slope, submarine fan, and basin plain settings. Aside from their potential as reservoir sands, mud-prone VTBT facies, in particular, have potential as deepwater source rocks, as unconventional reservoirs for shale-oil and shale-gas and, in some cases, as reservoir seals.

Following pioneering works of Kuenen (Kuenen & Migliorini, 1950; Kuenen & Menard, 1952), Bouma (1962), and Walker (1965), many studies have improved the overall understanding of turbidites from their depositional process to resultant geometry,

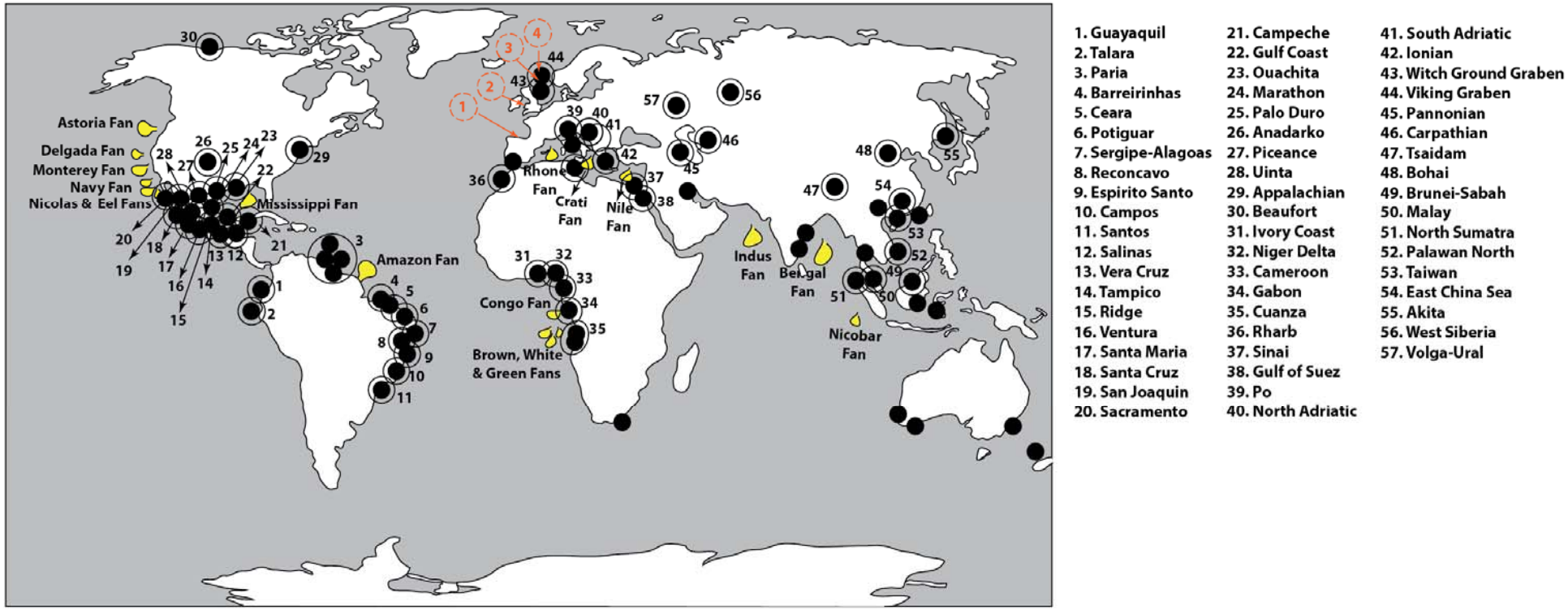

Figure 2.1. A sketch map of the world showing distribution of major hydrocarbon productive basins (black outlines without infill pattern) with turbidite fields (black dots), and some submarine fans (yellow) that have been widely studied. Many of these studies however, did not provide adequate information to better understand connectivity of TBT/VTBT facies, unlike their thicker-bedded counterparts. Information used for this figure was sourced from Bouma et al. (1985) and Pettingill (1998). Orange arrows mark locations from where data used in this research were sourced (1) Zumaia Section (Northern Spain), (2) Aberystwyth Grits Group (Mid Wales), (3) Pierce, Starling, and Fram Fields (United Kingdom North Sea), and (4) North Brae Field (United Kingdom North Sea).

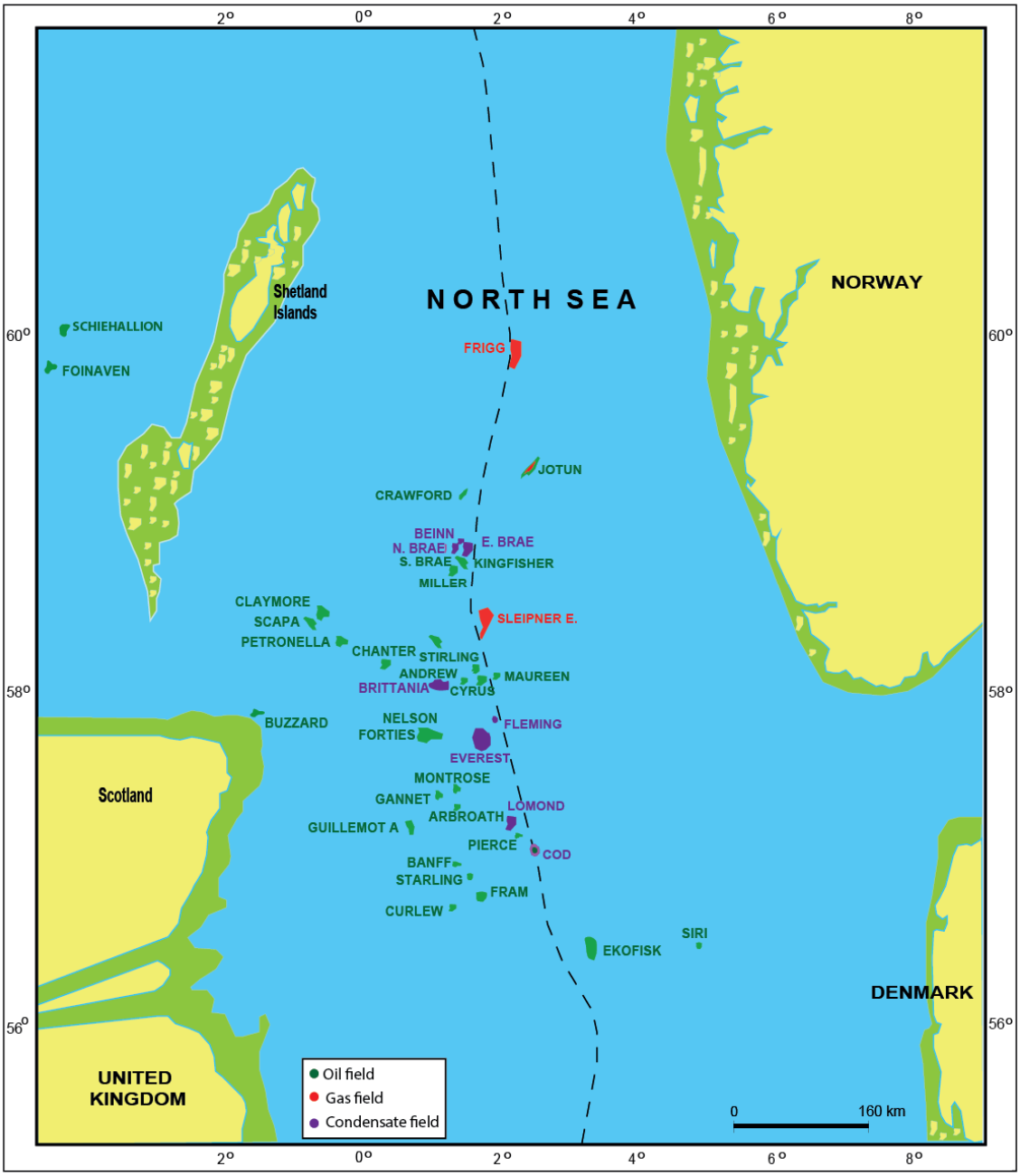

Figure 2.2. Schematic view of selected North Sea fields that have deepwater turbidite reservoirs. Many of these fields are mature and have oil bypassed or trapped within TBT/VTBT intervals. The bypassed oil, if economically produced, would help to delay decline in oil production rate, optimise oil recovery, and extend field life. Map was modified from http://arabcooking.me/map-uk-oil-fields.html

internal character, and reservoir architecture (Nilsen, 1984; DeVries & Lindholm, 1994; Pickering et al., 1995; Smith, 1995; Pirmez et al., 1997; Galloway, 1998; Normark et al., 1998; Richards & Bowman, 1998; Plink-Bjorklund et al., 2001; Deptuck et al., 2003; Gervais et al., 2004; Baas et al., 2005; Cavuoto et al., 2007; Hubbard et al., 2007a; Hubbard et al., 2007b; Wynn et al., 2007; Deptuck et al., 2008; Kane et al., 2009; McHargue et al., 2011; Romans et al., 2011; Sylvester et al., 2011; Sumner et al., 2012; Alpak et al., 2013; Grundvag et al., 2013; Pickering et al., 2015). Many of these studies, however, focused primarily on thick and very thick-bedded turbidites, leaving TBT and VTBT relatively less studied. There is now a growing volume of literature available on TBT/VTBT, which concerns description of their facies characterisation in a variety of sedimentary basins, internal arrangements of small-scale sedimentary structures, mode of transport, depositional patterns, and their depositional environments (Mutti, 1977; Stow, 1977; Stow & Bowen, 1978; Stow, 1979; Stow & Bowen, 1980; Stow & Shanmugam, 1980; Stow, 1981; Stow et al., 1982; Piper & Normark, 1983; Gorsline, 1984; Stow et al., 1984a; Stow et al., 1984b; Stow & Piper, 1984; Stow et al., 1984c; van Weering & van Iperen, 1984; Piper & Stow, 1991; Bouma, 1992; Stow, 1994; Stow et al., 1996; Busch & Brister, 1997; Piper & Deptuck, 1997; Pirmez et al., 1997; Stow, 2000; Normark et al., 2002; Gervais et al., 2004; Stow et al., 2012).

Despite the volume of literature available on TBT/VTBT facies, their consideration in the petroleum context has been much less considered. In particular, their lateral and vertical connectivity within their respective facies, and with thick-bedded turbidites and other deepwater facies remains unclear. The whole area of TBT and VTBT facies, their reservoir potential and internal connectivity is largely uncharted territory that appears not to have attracted as much research interest as the thick and very thick-bedded turbidites (King, 1990; Mijnssen, 1997; Friedmann et al., 2003; Larue & Friedmann, 2005; Larue & Hovadik, 2006; Hovadik & Larue, 2007; Manzocchi et al., 2007; Hovadik & Larue, 2010; Richards et al., 2010; Funk et al., 2012). This is partly because it is only during late-phase production, in many mature turbidite fields, that any attention is given to TBT/VTBT sands, when the desire to produce unswept oil trapped in the low-pay intervals becomes economically justified. This chapter, therefore, seeks to articulate what we do know about deepwater turbidites with emphasis on TBTs and VTBTs.

2.2 DEFINITION

The sedimentological definition of thin beds is 3-10 cm (0.03-0.1 m) thick, while very thin beds are <3 cm (<0.03 m) thick. Where <1cm (0.01 m) thick, a very thin bed is commonly referred to as a lamina (or lamination) (Stow, 2005). Industry terminology for TBT, however, is less restrictive of bed thickness and can be used to refer to turbidites below wireline-log resolution (<0.3 m approximately) or to the generally thinner-bedded turbidites associated with the thick sandstones of the main reservoir. Many turbidite events are represented by beds with a sandstone-siltstone lower unit grading upwards into a muddy upper unit, with a sharp to gradational boundary between the two. The turbidite thickness is, therefore, that of the complete sand-mud event. However, for the petroleum industry, there is a greater focus on the sand thickness rather than the actual turbidite event thickness.

For these reasons, the sedimentological definition of bed thickness is modified in this thesis (Figure 2.3). Furthermore, it should be recognised that any such definitions are simply placing artificial boundaries on a natural continuum of process and deposit for the purpose of better scientific description and understanding.

TBTs are here defined as having a sandstone-siltstone unit 0.03-0.1 m thick. They are the thinner bedded variety of sand-mud turbidites, generally deposited from fully evolved, medium to low-density waning turbidity currents in the uniform-depletive modes of the Kneller time-space matrix (Kneller, 1995). They are best represented by the classic Bouma facies model (Bouma, 1962) and its full range of variations (see section 2.4).

VTBTs are here defined as having a siltstone-sandstone unit <0.03 m thick. They are typical of ‘tiger-stripe’ and shale-rich successions, generally deposited from fully evolved, low density turbidity currents under a variety of conditions. They are best represented by the Stow facies model (Stow & Shanmugam, 1980) and its variations (see section 2.4).

2.3 PROCESS OF DEPOSITION

2.3.1 General understanding of turbidity currents

Turbidity currents are one of the most important ways by which fine, medium and coarse-grained material is transferred from shallow to deep water. They are one of a family of

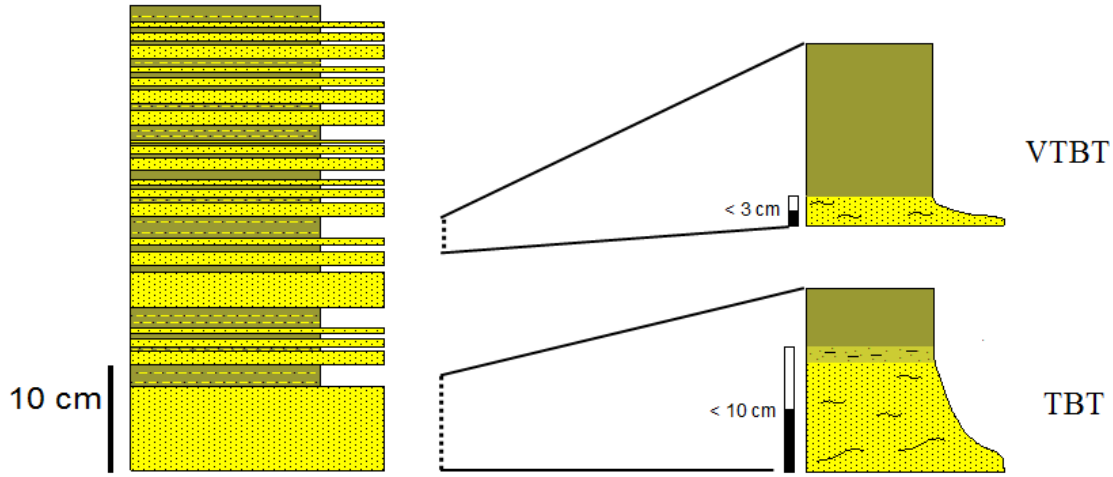

Figure 2.3. Definitions of thin-bedded turbidites (TBTs) and very thin-bedded turbidites (VTBTs). Note that the thickness of the sand/silt basal part of the turbidite is taken as the measure of 'bed' thickness.

downslope and related processes as illustrated in Figure 2.4 (Stow et al., 1996; Hüneke & Mulder, 2011; Talling et al., 2012; Hansen et al., 2015; Pickering & Hiscott, 2016). They are commonly turbulent suspensions of mud and sand (and gravel in some cases) in water, which are propelled by the downslope component of gravity acting on the excess density. They may occur as short-lived surge events that travel for only a matter of kilometres downslope, or go through a process of flow ignition such that an autosuspension process is generated in the flow. This permits very long distance transport over tens to several thousands of kilometre, both downslope and across flat abyssal plains. They can even travel a certain distance in an upslope direction before they come to a halt by a combination of frictional resistance, loss of sediment from the base of the flow and reverse gravitation pull.

Individual turbidity currents are discrete events with very variable recurrence intervals (10^0-10^5 y) and of very different volumes. The largest flows are known to overtop channel margins of >850 m in height (Dorrik Stow, personal communication, 2015). These are likely to be several kilometres in width and probably tens of kilometres in length. Much smaller turbidity currents also occur. Such currents can be channel confined or flow across open slopes with little apparent confinement. They can deposit beds between <0.01 m and >10 m in thickness. Mean accumulation rates, therefore, are also very variable, typically from 0.1 m to >1 m/ky. The frequency of occurrence of turbidity currents ranges from 1/1000 years (approximately) for the distal Bengal fan, to one every few years for parts of the Amazon and Congo fan systems, or more frequently still offshore active rivers and in some lacustrine environments (Dorrik Stow, personal communication, 2015).

2.3.2 Flow concentration

Turbidity currents occur at a range of sediment concentrations, from those that are considered high-concentration flows or high-density turbidity currents, HDTs (Lowe, 1976; Lowe, 1982) at around 50-250 kg/m^3, to low-concentration flows (or low-density turbidity currents, LDTs) of around 0.25-50 kg/m^3 (Stow & Bowen, 1980; Stow et al., 1996; Pickering & Hiscott, 2016). There is some debate around the upper and lower limits of turbidity current concentration, such that hyperconcentrated flows are taken as ranging upwards from around 450 kg/m^3 and debris flows upwards from around 800 kg/m^3. Hyperpycnal underflows from rivers in flood typically have concentrations in the

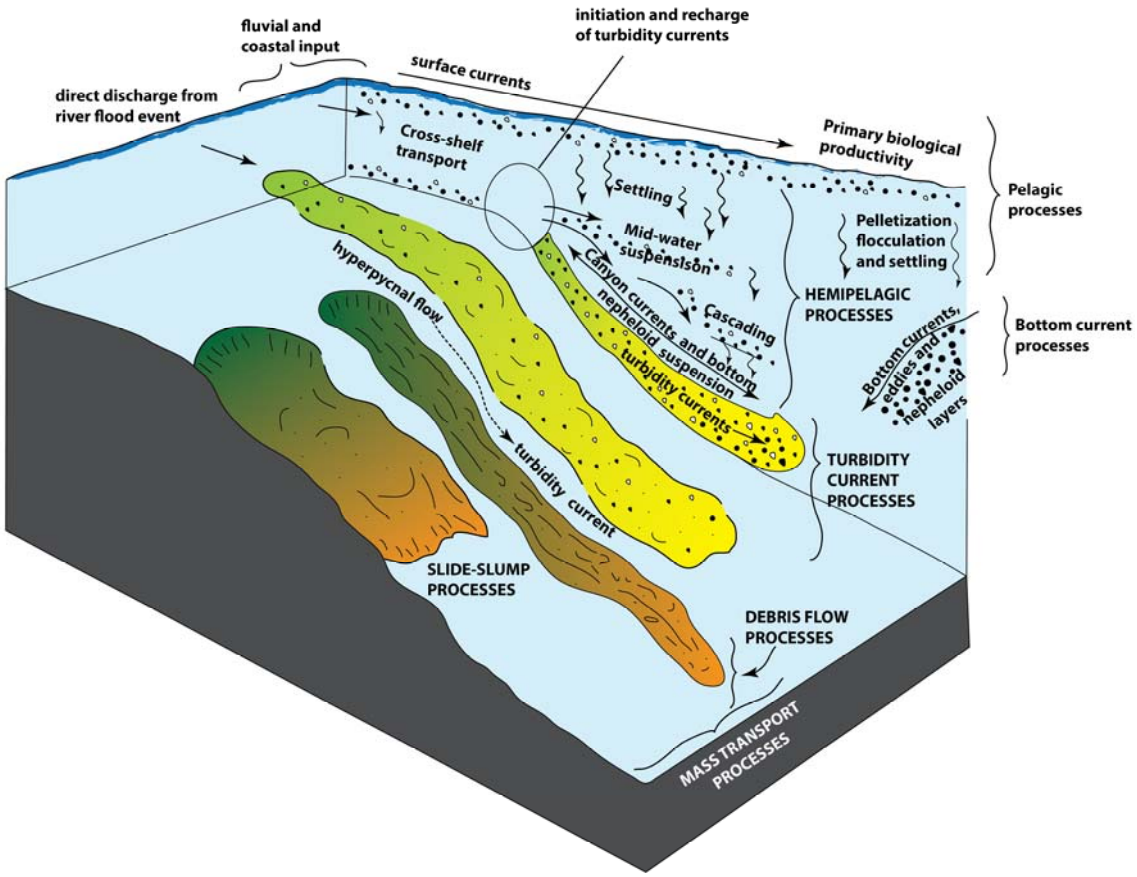

Figure 2.4. Deepwater process family including downslope, along slope, and hemipelagic processes (modified from Stow & Mayall, 2000).

upper range of low-concentration turbidity currents, whereas bottom current concentrations (depositing contourites) are several orders of magnitude lower – around 0.00002-0.002 kg/m^3 (0.02-2 mg/l) (Stow et al., 2009).

The high-concentration flows are typically bi-partite, having a lower traction carpet with very high concentration (hyperconcentration), grain interaction and quasi-viscous flow behaviour especially near the base of the flow, and a fully turbulent more dilute upper part (Postma et al., 1988; Middleton, 1993; Stow et al., 1996; Hallworth & Huppert, 1998; Parsons et al., 2006). These HDTs are highly competent, can transport coarse grain sizes (coarse sand and gravel) and give rise to *coarse-grained turbidites*, including thick sandy turbidites, mega-turbidites, and deepwater massive sands (Kneller & Branney, 1995; Stow & Johansson, 2000). Such deposits are mostly thick and very thick-bedded and are discussed by Cronin et al. (in press).

Low-concentration flows are, for the most part, fully turbulent Newtonian flows and capable of carrying sand, silt and clay-sized material (Dott, 1963; Middleton & Hampton, 1973; Mansfield, 1985; Middleton, 1993; Altinakar et al., 1996; Hallworth & Huppert, 1998; Baas et al., 2004; Choux et al., 2005; Parsons et al., 2006; Talling et al., 2007; Piper & Normark, 2009; Talling et al., 2012; Hansen et al., 2015; Shanmugam, 2016). The largest grain size transported is a reflection of the flow competency, density and velocity. These LDTs deposit *medium-grained turbidites* and *fine-grained turbidites*, which are mostly medium and thin-bedded.

Turbidity currents become progressively more dilute as more and more of the suspended sediment load is deposited. In its final stages the turbidity current and any remaining suspension begins to mix upward into the water column forming a very dilute suspension cloud many hundreds of meters above the seafloor (Stow et al., 1990; Stow & Wetzel, 1990). This process has been termed reversing buoyancy (Sparks et al., 1993) and the deposits called *hemiturbidites* (Stow & Wetzel, 1990).

2.3.3 Flow velocity and deposition

Flow velocity of turbidity currents has been measured directly in only very few cases (Postma et al., 2009; Janocko et al., 2013; Sumner et al., 2013; Pickering & Hiscott, 2016; Postma et al., 2016; Azpiroz-Zabala & Cartigny, 2017; Symons et al., 2017). It has been calculated more commonly by measuring the time between sequential cable breaks that lie across the seafloor in the path of such currents. Indirect determination of flow velocity

is more readily made from the nature of bedforms generated by the passing current and from the maximum clast size present in the deposited turbidite beds. Summarising these data yields the velocity/grain size matrix for turbidity currents, illustrated in Figure 2.5. Whereas the high-concentration flows depositing coarse-grained turbidites can reach velocities in excess of 20 m/s, those that are in the depositional phase for medium and fine-grained turbidites have slowed to around 0.5 m/s and 0.15 m/s, respectively. Figure 2.3 also shows the best estimates of the time taken for individual turbidite beds to be deposited – from minutes to days.

Deposition occurs from the base of the turbidity current as the flow loses its carrying capacity (or competence). This is the result of (a) a decrease in flow velocity, (b) a reduction in flow density, (c) interaction with a bottom current flow across the path of the turbidity current, or (d) progressive loss of sediment due to deposition. In reality, deposition is most likely due to a combination and interaction of these different factors, influenced by topographic change and frictional resistance of the seafloor. A gradual decrease in flow competence at any one location results in the deposition of a normally graded bed.

Deposition occurs through a boundary layer in which there is locally increased shear stress caused by the friction between the flow and the seabed. This affects the final characteristic of the grading and sedimentary structures within the turbidite. Stow and Bowen (1978; 1980) showed how the shear sorting mechanism yields silt-mud lamination in TBTs. It is proposed here that the same mechanism is involved in the production of normal parallel lamination in fine sandstones.

2.3.4 Flow initiation

The causal mechanisms for the origin of turbidity currents are widespread and varied. One principal cause is the failure of submarine slopes leading to sliding, slumping or debris flow processes. These may evolve through ingestion of ambient seawater into turbidity currents. Slope failure, commonly linked with development of excess pore water pressure within the sediment pile, can be caused by: (a) seismic activity, (b) sea-level rise and fall, (c) excessive sediment loading, (d) gas hydrate instability and release, and (e) changes in groundwater flow conditions within the slope and shelf (Lee, 2009; Twichell et al., 2009; Hüneke & Mulder, 2011; Talling, 2014; Pickering & Hiscott, 2016).

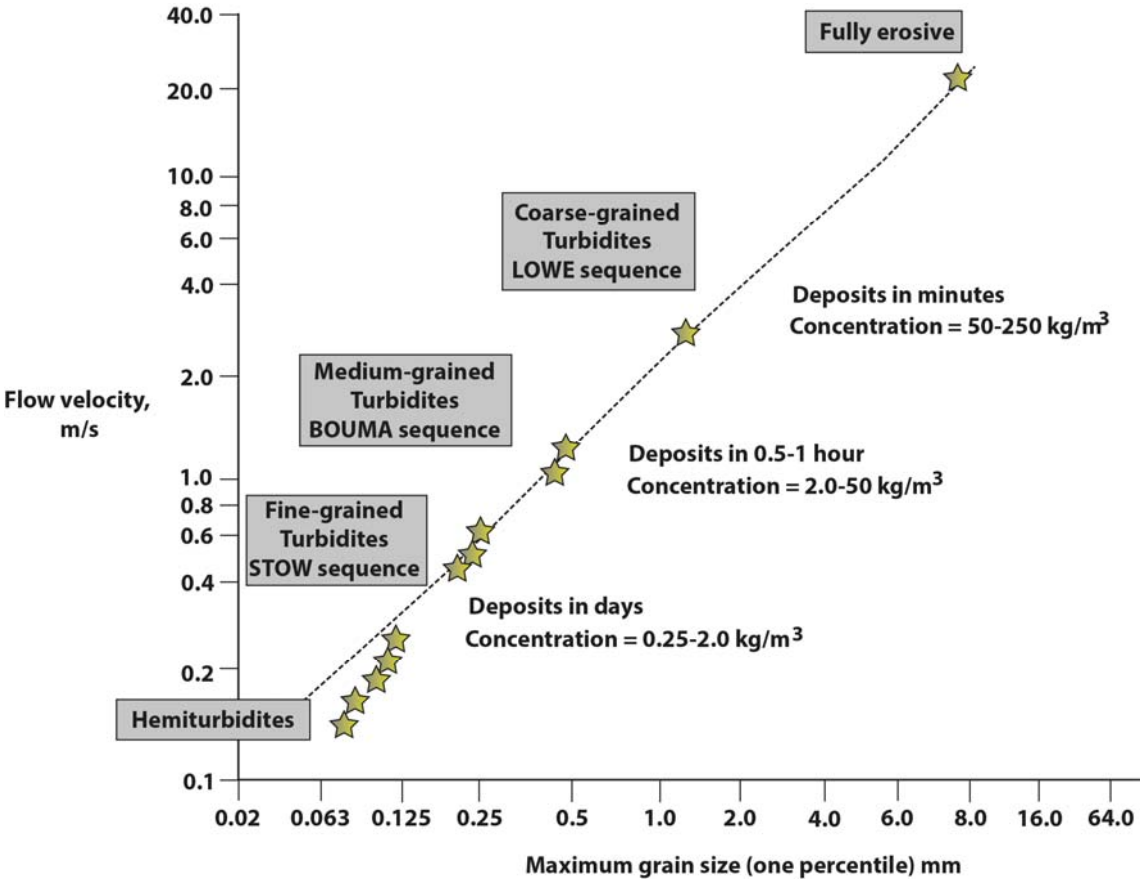

Figure 2.5. Velocity-grain size matrix for turbidity currents (modified from Stow et al., 2009).

Other factors more specific to the generation of low-concentration turbidity current include: (a) sudden excess sediment supply by rivers in flood (i.e. their generation from hyperpycnal flows); (b) rapid glacial discharge events; (c) re-suspension of shelf edge to upper slope sediment as a result of storm stirring and the incidence of internal tides/waves; and (d) storm build-up of water across a continental shelf and its rapid discharge down submarine canyons.

The principal modes of initiation, remoulding, transport and deposition by turbidity currents are summarised in Figure 2.6.

2.4. STANDARD FACIES MODELS

Turbidites have been one of the better known and most intensively studied deepwater sediment facies since they were first recognised in the 1950s (Kuenen & Migliorini, 1950) and the first facies model developed by Bouma (1962). They are now very well-known from sediment cores recovered from modern deepwater systems, subsurface (hydrocarbon) boreholes, and ancient outcrops now exposed on land. Each new study of a particular turbidite system reveals specific deposit characteristics and facies for that system. The most commonly observed facies have been variously synthesised into a range of facies schemes proposed by Mutti and Ricci Lucchi (1972), Stow (1986), Ghibaudo (1992), Mutti (1992), Stow (1994), Pickering et al. (1995), Mulder and Cochonat (1996), Stow et al. (1996), Mutti & Tinterri (2000), Hüneke and Mulder (2011), among others.

These composite characteristics and multiple datasets have been synthesised into facies models for coarse-grained turbidites (Lowe, 1982; Stow & Mayall, 2000; Haughton et al., 2009), medium-grained turbidites (Bouma, 1962; Walker, 1965), and fine-grained turbidites (Stow, 1977; Piper, 1978; Stow & Shanmugam, 1980). For convenience, these are referred to as the Lowe, Bouma and Stow sequences or facies models, after the authors who first established the scheme. Each of these facies models shows a characteristic sequence of sedimentary structures and grading that reflect deposition from a single turbidity current event. They are event deposits. The different structures are referred to as divisions within the sequence. The Stow sequence is more or less equivalent to the D-E divisions of the Bouma sequence, or to the E1-3 divisions of Piper (1978).

The complete sequences are present in <10% of turbidites. More common are partial sequences in which the same order of divisions is preserved but not all are present

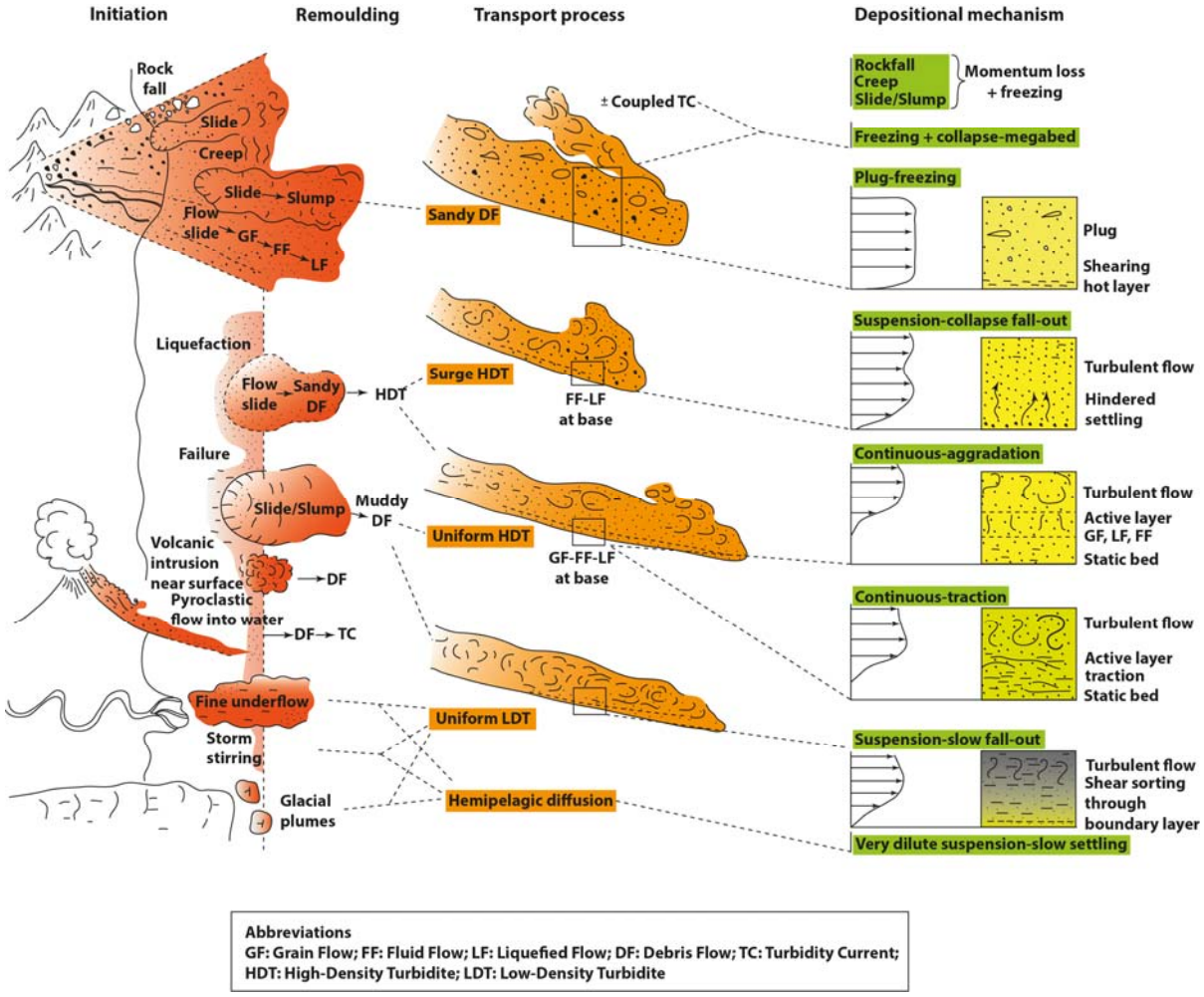

Figure 2.6. Turbidity current and related downslope processes: initiation, remoulding, transport and depositional phases (Stow et al., 1995a; Stow et al., 1996).

in any one bed. For each sequence, the lower divisions represent deposition from the current when it is more energetic and the upper divisions when it is less energetic. For a single turbidity current, this can be achieved from more proximal to more distal, respectively, and also from channel axis to overbank. The same high to low energy regime applies to Lowe, Bouma and Stow turbidites. In some cases Lowe divisions are overlain by Bouma divisions in a single bed, or Bouma divisions by Stow divisions. Rarely, all three can occur in megaturbidites.

Thin-bedded and medium-bedded turbidites are best characterised by the Stow and Bouma models. These are shown, together with the typical range of partial sequences in Figures 2.7 and 2.8. They represent deposition from uniform turbidity currents in the depletive regime of the Kneller-Branney matrix. They are the most abundant and widespread types of turbidite in both marine and lacustrine settings. Modern and ancient examples of TBTs and VTBTs are shown in Figure 2.9. Thick-bedded/coarse-grained turbidites are discussed by Cronin (in press).

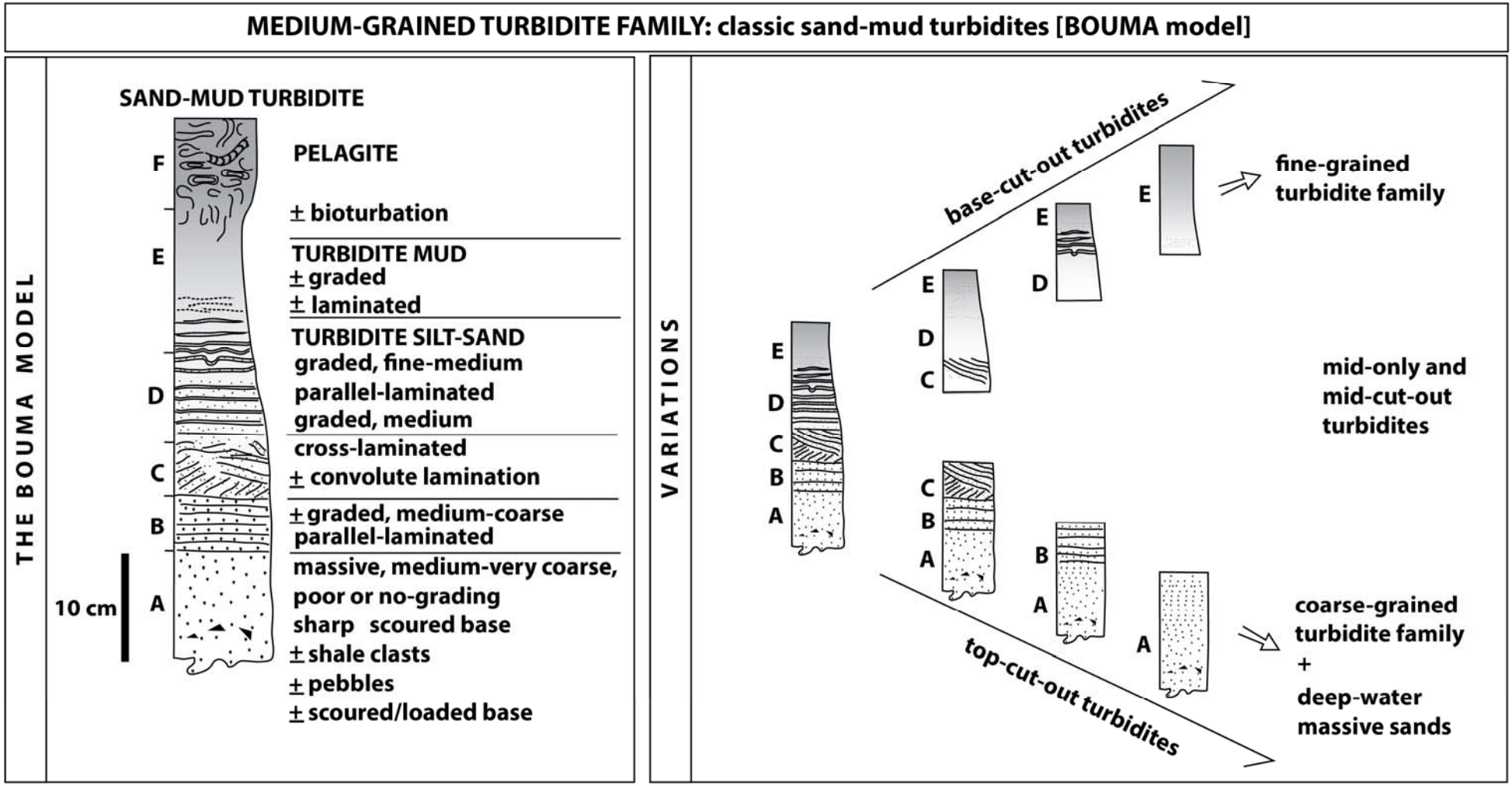

Figure 2.7. Facies model for medium-grained (Bouma) turbidites and partial-sequence variations. Typical of thin-bedded turbidites.

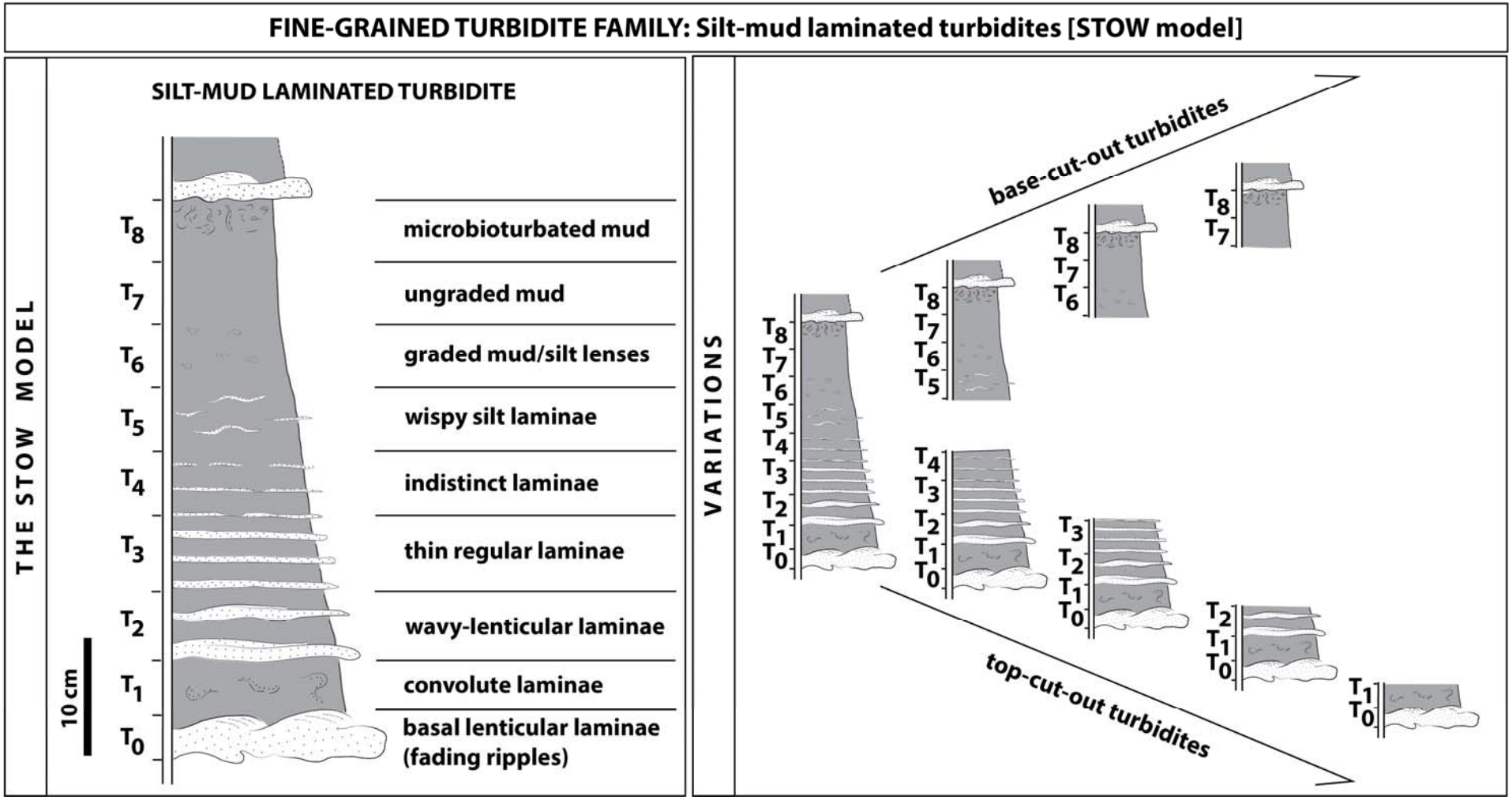

Figure 2.8. Facies model for fine-grained (Stow) turbidites and partial-sequence variations. Typical of very thin-bedded turbidites.

A.

B.

Figure 2.9. Selected photographs of VTBT facies from outcrop (A and B), Silurian Trefechan Formation, Aberystwyth Grits Group, Mid Wales. Note distinctive faded-ripple basal divisions (Stow T_0). The lower bed in 'B' is composed of disorganised VTBT.

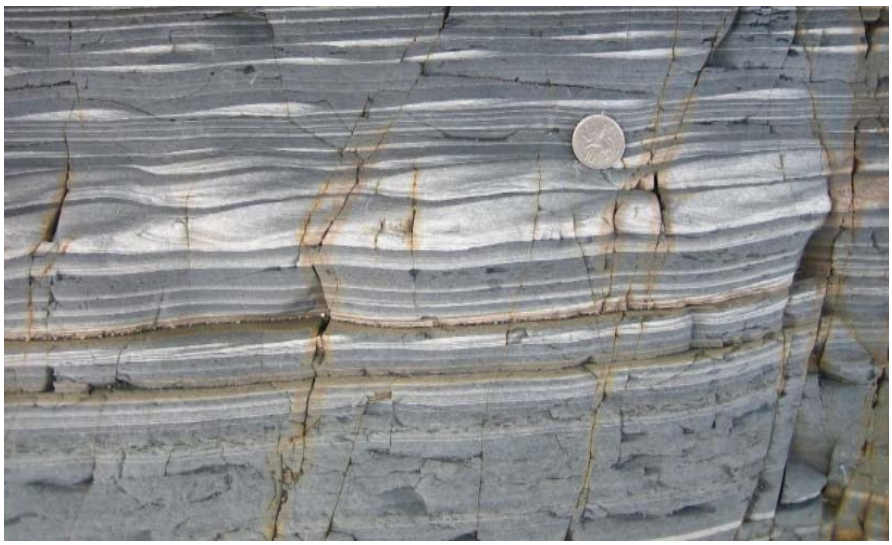

C.

D.

Figure 2.9 continued. Selected photographs of (C) low net-to-gross VTBT facies, Silurian Trefechan Formation, Aberystwyth Grits Group, Mid Wales, and (D) very high net-to-gross TBT/VTBT facies, Eocene turbidite succession of the Itzurun Formation, exposed at Zumaia, Northern Spain. While the VTBT facies in 'C' above are dominated by faded ripples, and parallel/ripple, the TBT/VTBT facies in 'D' are characterised by remarkable lateral continuity of beds, monotonous fabric, few ripples, and planar bedding with regularity of bed thickness.

E.

F.

Figure 2.9 continued. Selected photographs of (E) TBT facies interbedded with VTBTs and some medium-bedded turbidites, Eocene turbidite succession of the Itzurun Formation, exposed at Zumaia, Northern Spain. Some of the TBT facies are characterised by parallel lamination (Bouma division B) with pervasive current ripples, which indicate deposition in lower energy regimes, typical of Bouma division C (F).

G.

H.

Figure 2.9 continued. Selected photographs of TBT and VTBT facies from outcrop showing TBT facies with interbeds of VTBTs and medium-bedded turbidites. In 'G' above (Silurian Mynydd Bach Formation, Aberystwyth Grits Group, Mid Wales), lenticular lamination is evident, in addition to parallel continuous bedding and cyclicity of beds. Internal structures are dominated by current ripples and planar continuous-wavy lamination. The low net-to-gross facies in 'H' (Zumaia section, Eocene Itzurun Formation, Northern Spain) are dominated by VTBTs with TBT interbeds. The section is marked by wavy-planar continuous lamination.

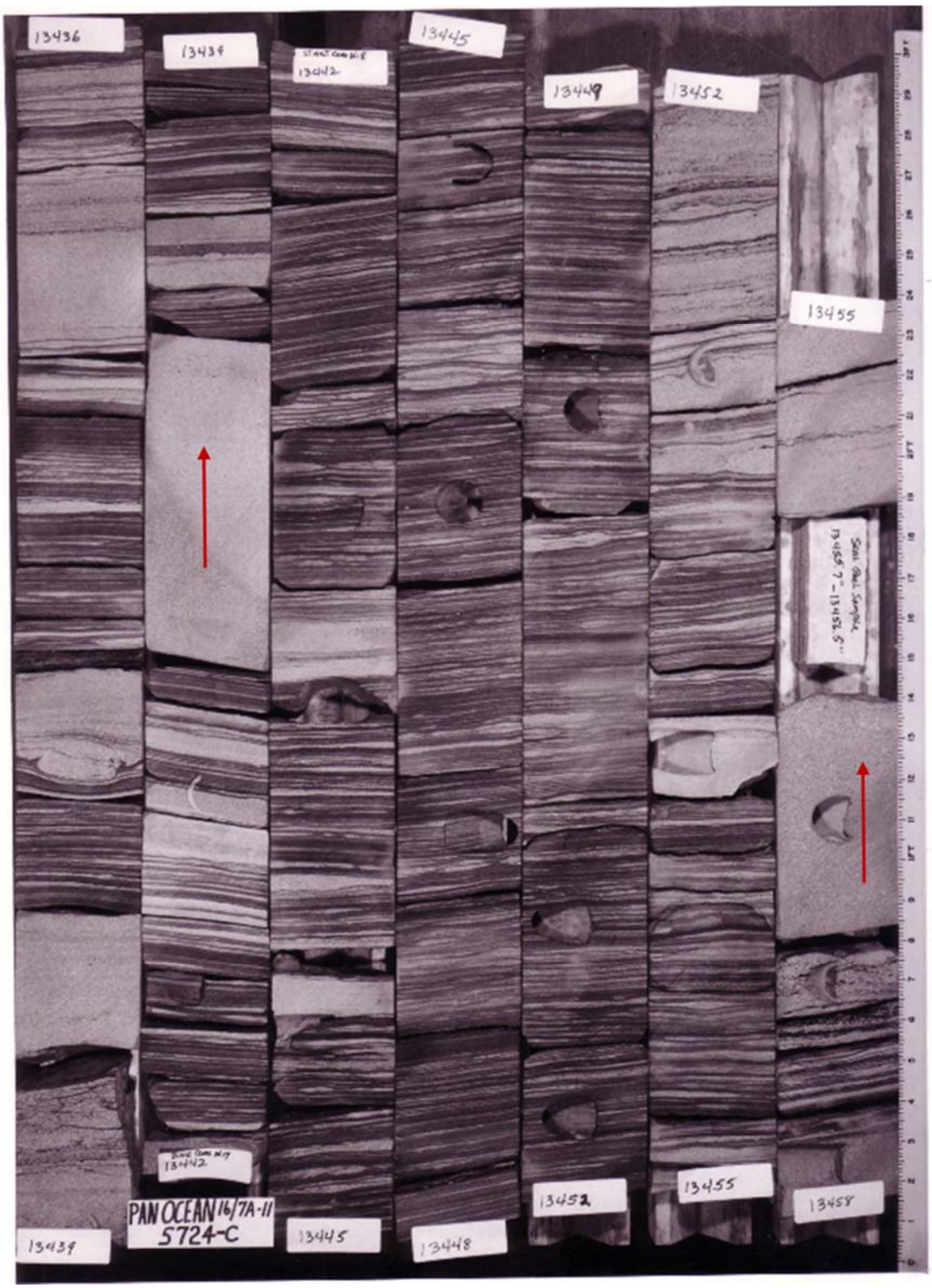

I.

Figure 2.9 continued. Selected photograph of TBT/VTBT facies from the North Brae Field, North Sea, Upper Jurassic. The interval comprises two medium-bedded interbeds (red arrows). Disturbed laminae, lenticular-wavy laminae, current ripples, distinct-indistinct laminae, and wispy laminae are some of the internal structures that are evident.

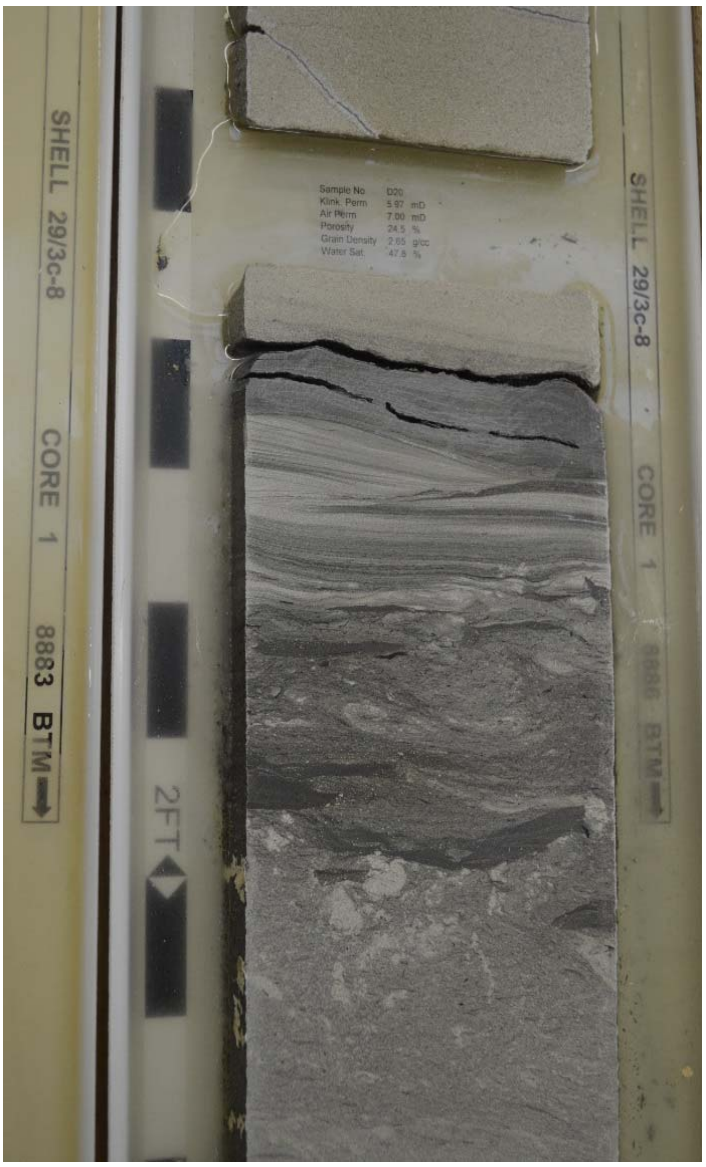

J.

Figure 2.9 continued. Typical Forties Formation core, North Sea, Lower Tertiary, showing sandy base of TBT (upper), VTBT with $T_{0\text{-}2}$ divisions (middle), and disorganised TBT (lower). The disorganised part is typified by a chaotic fabric.

K.

Figure 2.9 continued. Clarach section, Silurian Trefechan Formation, Aberystwyth Grits Group, Mid Wales, showing typical basinal succession of TBTs, VTBTs and medium-bedded turbidites. Vertical variation of bed-thickness characterised by oscillation sequences of around 2-3 m thickness mark the 16-m cliff section.

L.

Figure 2.9 continued. Tabernas Basin succession, Chozas Formation, Miocene, South-East Spain, with TBTs and VTBTs (middle left) within a submarine channel, incised by conglomeratic debrite and medium to thick-bedded sandstone turbidites. Section above dry river-bed (foreground) is approximately 3 m.

2.5 CONNECTIVITY

For any depletion strategy by water injection to result in economic oil recovery, there must be connectivity between the injection wells and the production wells. The effectiveness of these connectivity pathways or flow conduits depends on the proportion of sand that is in direct connection with other sand.

The term connectivity in the literature is somehow ambiguous (King, 1990; Mijnssen, 1997; Stephen et al., 2001; Larue & Hovadik, 2006; Hovadik & Larue, 2007; Manzocchi et al., 2007; Hovadik & Larue, 2010; Richards et al., 2010; Villamizar et al., 2015). Larue and Hovadik (2006) define sandbody (or geobody) connectivity as the percentage of the reservoir that is connected and, reservoir connectivity as the percentage of the reservoir that is connected to wells. Hovadik and Larue (2010), following Larue and Hovadik (2006), identify two kinds of connectivity, bulk reservoir connectivity and reservoir to well connectivity. According to these authors, bulk reservoir connectivity is characterised by the connected sand fraction that is either expressed as a ratio of the biggest geobody volume to the volume of the grid or ratio of the biggest geobody volume to the volume of all reservoir geobodies.

In addition, the authors recognise reservoir to well connectivity as the fraction of reservoir flow units that are connected to one another within a completed well interval. However, these definitions have been fraught with pitfalls. First, the reservoir connectivity yields typically high connectivity at high net-to-gross (Hovadik & Larue, 2010), whilst the reservoir to well connectivity is computed using geostatistical models that are developed by varying continuity lengths (variogram-based), and/or stochastic realizations, by varying model seed number. Based on these critical pitfalls, some of these authors (Larue & Hovadik, 2006; Manzocchi et al., 2007; Hovadik & Larue, 2010) recognise the limitations in their concepts, and consequently, stressed the need to compute connectivity, bearing in mind its sensitivity to geological situations that vary from place to place within the reservoir.

The Sand Connectivity Index (SCI)-derived connectivity developed and applied in this thesis differs from the previous concepts of connectivity in that it is calculated using parameters (i.e. geological attributes) that are primarily extracted from cores, and by extension, from reservoir models that are built using geologically consistent stratigraphic architecture, rather than stochastically-generated (i.e. geostatistically-derived), geologically inconsistent models. Connectivity of reservoir sandbodies is a function of distance (Larue & Hovadik, 2006). The SCI concept of connectivity

recognises lateral and vertical variations in geological attributes of turbidite reservoir facies from one facies association to another, within a particular turbidite reservoir interval. Apart from its sensitivity to these variations, it quantifies connectivity in sandstone-rich and sandstone-poor facies associations because the sandstone-poor facies can still create sweep zones that can be targeted using secondary recovery mechanism such as gas or water injection, or better still by tertiary recovery methods such as polymer flooding. The variation in connectivity over a particular reservoir interval, is captured by a combination of geological attributes that are further developed into lateral and vertical components of the SCI. These components are computed at selected distances away from the producer well (16/07a-B1, Chapter 7; 16/07a-B8, Chapter 8). This enables SCI-derived connectivity to be defined as a function of distance from a particular reference location or well.

The quantitative approach developed in my research and presented in this thesis recognises, like in previous work, the close relationship between net-to-gross and connectivity. This relationship is further explored in Chapter 7 of this thesis. However, unlike in previous work, a threshold in net-to-gross is set using percolation theory. Below this threshold, connectivity approaches zero, and above the threshold, it is non-zero (King, 1990; Hovadik & Larue, 2007; Hovadik & Larue, 2010). The SCI approach reveals that connectivity is non-zero even at lower net-to-gross, except at critical value of net-to-gross (Chapter 7). This is possible because in any interval with sand beds, there is a measure of continuity, which can be expressed in terms of lateral and vertical connectivity indices, and thus, have a measure of connectivity.

The approach to vertical connectivity (initially referred to as SCI) was developed using core data from four wells in the North Brae Field. The results are presented in Chapter 4. Because of the remarkable regularity of bedding, sheet-like geometry, and high degree of continuity of beds, a basin-plain turbidite succession in the Eocene section of the Itzurun Formation, exposed at Zumaia (Basque Country, Spain), was chosen for outcrop attribute data gathering. These data were used to fully develop the SCI (Chapter 6). The SCI approach was developed for selected TBT/VTBT facies association intervals, varying in geological attributes (Chapter 3). The results were compared quantitatively, and modelled at high resolution for flow simulation studies, in order to investigate the effects of these variabilities (also termed sedimentary heterogeneities) on oil recovery and reservoir flow performance. In addition, the SCI-derived connectivity approach was applied to study the connectivity bridge between the southern lobe and the central channel

in the North Brae Field (Chapter 5), with a view to providing better understanding of the impacts of variable connectivity, between a producer well and an injector well, on reservoir flow performance.

PART 2

DATABASE AND METHODS

Chapter 3

Database and Methods

Photo by Bayonle Omoniyi

Sheet thin-bedded-to-very thick-bedded turbidites
Silurian Mynydd Bach Formation
Aberystwyth Grits Group
Ceredigion (Mid Wales), UK

This chapter focusses on the data and a range of methods used for this research. In particular, it discusses the 'attribute indices' method, and basic principles and techniques that underlie core-based porosity and permeability measurements, reservoir modelling, and flow simulation as used in this thesis. References have been collated at the end of the thesis.

3.1 DATABASE

3.1.1 Core

For this research, cores revered from nine wells in the North Brae Field, United Kingdom Continental Shelf of the North Sea, were studied. These wells have high core recovery (average, 75-100%), and cored intervals comprise TBT/VTBT proportions that range from 10% (e.g. 16/07a-B1) to 100%. In the nine wells, a total of 5,851 ft (1,783.4 m) were logged and described, of which 1,107 ft (337.4 m) was logged at 1:10 scale for a more detailed study (Chapter 4). In addition to the cores from the North Brae Field, 16,275 ft (4,960.6 m) of cores were logged and described from eighteen wells covering Pierce, Starling, and Fram Fields, United Kingdom Continental Shelf of the North Sea. The data provided geological attributes of TBT/VTBT facies within a typical channelised setting (Pierce Field), proximal lobe setting (Starling Field), and distal lobe setting (Fram Field). In total, 22,126 ft (6,744.0 m) of cores were logged for this research and the insights gained were built into this thesis, particularly, Chapters 2, 4 and 8.

It is important to note that the cores from the North Brae Field were provided by Marathon Oil Company, and those from Pierce, Starling, and Fram Fields were provided by Shell Oil Company. Both companies are located in Aberdeen, United Kingdom. Other cores from the North Brae Field were studied at the National Core Repository, Keyworth, United Kingdom (Figure 3.1; A, B).

3.1.2 Outcrop

Outcrop studies offer invaluable insight into the impact of (sedimentary) heterogeneities on fluid flow (Prosser & Carter, 1997; Slatt et al., 1998; Browne & Slatt, 2002; Larue, 2004; Sullivan et al., 2004; Pedersen et al., 2007; Labourdette et al., 2008; Davis et al., 2010; Funk et al., 2012; Amy et al., 2013; Eschard et al., 2014; Pickering et al., 2015). Two major fieldwork programmes were undertaken to help build a robust attribute database for TBT/VTBT facies in ancient systems. The first was a comprehensive 25-day fieldwork programme in Mid Wales, United Kingdom, covering Trefechan Formation and Mynydd Bach Formation, both in the Silurian Aberystwyth Grits Group. The two formations consist of deepwater turbidite sandstones in addition to some shallow marine deposits. In Mynydd Bach Formation, turbidite sandstones comprise thick-bedded and largely, structureless sandstones, with interbedded TBT/VTBT facies and

A.

B.

Figure 3.1. Selected photographs showing (A) core shelves, National Core Repository, BGS, Keyworth, and (B) a typical core study section. Study of beds with thickness ranging from <1cm to 10 cm can be very challenging indeed. For this research, a total of 22,126 ft (6,744 m) of cores and over 892 ft (272 m) of outcrops were logged for this research, totalling 23,018 ft (7,016 m). To put in context, the total section logged for this research covers the length of 78 standard football pitches.

turbidite mudstones. Trefechan Formation, conversely consists of interbedded mudstones and sandstones that are largely thin-to-very thin-bedded (Figure 3.2). The deep understanding gained from the preliminary interpretation of results provided significant information about the general characteristics of TBT/VTBT, especially on the subject of their attributes and attribute indices (Chapters 2, 3, 6 and 8), and were used to inform the geometrical parameters upon which the related facies models were constrained (Chapters 5 and 7). The complete preliminary results are set aside for future research purposes, but the sedimentary logs are provided in Appendix A.

The second fieldwork programme was undertaken in Zumaia, a village in the Basque Country, Spain. The 5-week intensive fieldwork was scheduled to develop the Lateral Connectivity Index (LCI), the lateral component of the Sand Connectivity Index (SCI). Within this period of five weeks, approximately 597 ft (182.0 m) interval was logged and described. This interval constitutes the siliciclastic section of the Itzurun Formation (Figure 3.3). TBT/VTBT attribute data, including bed thickness data, were collected over the period of study. The bed thickness data collected are reserved for research in the future, but the attribute data were used to prepare the results presented in Chapter 6 of this thesis.

3.1.3 Wireline logs

Wireline logs, comprising gamma ray, neutron, density and sonic from ten wells in the North Brae Field (16/07a-B27, 16/07a-B14, 16/07a-B1, 16/07a-B7, 16/07a-B8, 16/07a-19, 16/07a-B17, 16/07a-B10, 16/07a-7) were studied for this research. To aid facies interpretation and well correlation, cores recovered from the wells were matched with wireline logs. Uncertainty in facies interpretation was significantly reduced by studying wireline logs from seven wells in Pierce and Starling Fields to delineate log character in TBT/VTBT intervals.

Figure 3.2. Deepwater turbidite succession at Clarach, Silurian Trefechan Formation, Aberystwyth Grits Group, Wales. The succession comprises interbedded turbidite mudstones and sandstone and are largely thin-bedded.

Figure 3.3. A photograph showing a deepwater turbidite succession (Eocene Zumaia section) in the Itzurun Formation, Basque Country, Northern Spain. Approximately 597 ft (182 m)-interval of this section was logged and described for this research.

3.2 METHODS

3.2.1 Turbidite attributes

The principal sedimentary attributes used to characterise and discriminate between different TBT/VTBT systems are listed below.

(a) Facies: nature of turbidite facies present; quantification of the relative proportion of TBTs with Bouma sequences and VTBTs with Stow sequences.

(b) Sedimentary structures: recognition of full and partial Bouma or Stow sequence types, and top/mid/basal divisions present.

(c) Facies associations: the grouping of TBT and VTBT facies in order to represent the succession (and parts of the succession) more succinctly than through individual facies; the associated facies present in succession and their relative proportion is also noted.

(d) Bed thickness: examination of bed thickness, including full turbidites (i.e. sand-mud graded beds); quantification of the mean thicknesses of sand and mud parts of beds.

(e) Vertical sequences of bed thickness: a broader perspective of the turbidite succession within mega- and meso-sequences, either from visual inspection or determined from statistical analysis; particular focus on the micro-sequences within the TBT/VTBT package.

(f) Sand-shale or sand-mud ratio: quantification of the relative proportion of sand and mud within a given sequence; this is a derivative measurement of the standard net-to-gross ratio used in the petroleum industry.

(g) Connectivity: characterisation/measurement of the sand and shale geometry, sand/shale lengths, and number of sands/silts in direct contact with one or more other sands/silts.

(h) Sediment texture: determination of the mean grain size of sands, mean grain size of silts, and mean grain size of the interbedded mud divisions; other textural attributes, in particular, sorting and skewness can also be quantified.

(i) Sediment composition: mineralogical and/or geochemical make-up of the different sediment fractions (sand/mud); siliciclastic, bioclastic, volcaniclastic, chemoclastic or mixed turbidite types.

(j) Sediment fabric: the alignment and disposition of individual grains and particles with respect to each other; applicable to both sand and mud fractions.

3.2.2 Attributes indices

The set of TBT/VTBT attributes discussed in previous subsection can be quantified using four fundamental variables, referred to as *attribute indices*. The indices were originally developed from cores recovered from nine wells in the North Brae Field, and later extended to wells in the Pierce, Starling, and Fram Fields within the Palaeocene Forties Formation, for complementary application. For calculating dimensionless attribute indices, bed thickness cut-off is 1cm.

3.2.2.1 *Facies* Net-to-Gross Index

The *facies* Net-to-Gross Index (NGI) recognises the distinctive TBT/VTBT facies within the constituent facies of a turbidite sequence. It particularly expresses the standard net to gross sand value commonly used to evaluate reservoir intervals, and indicates the relative proximality of deposition and/or energy and competence of turbidity current. It is calculated using Equation 3.1.

$$\mathrm{NGI} = \left[{(\mathrm{NT})_{\mathrm{f}}} \Big/ {(\mathrm{GT})_{\mathrm{f}}} \right] \tag{3.1}$$

$(\mathrm{NT})_{\mathrm{f}}$ and $(\mathrm{GT})_{\mathrm{f}}$ are net and gross thicknesses, respectively, for the particular facies association interval being considered.

NGI varies from 0 to 1. Low NGI values represent low net-to-gross for the facies association, whereas high NGI values indicate high net-to-gross.

3.2.2.2 Sand Connectivity Index

The Sand Connectivity Index (SCI) is a new approach developed to estimate spatial connectivity (also referred to in ensuing chapters as connectivity) in TBT/VTBT-associated deepwater architectural elements. Although pressure data, well-test data, and production data are all different ways of estimating connectivity, they indirectly indicate connectivity between fluid contacts (pressure data) or injector well to producer well (well test and production data). By contrast, the spatial connectivity indicated by Sand Connectivity Index (SCI) is an attribute index that provides a quantitative estimate of the connectivity between primary (turbidite) reservoir facies and associated TBT/VTBT facies. It is derived from the nature of bed/lamination cross-cutting relationships, and it serves as an important discriminator for predicting lateral and vertical continuity and connectivity in TBT and VTBT facies associations, and in related primary reservoir sands. It provides a more rigorous predictor of TBT/VTBT sand reservoir potential than conventional sand net to gross. SCI can be calculated from Equation 3.2.

$$\mathrm{SCI} = \frac{1}{2}(\mathrm{VCI} + \mathrm{LCI}) \text{ x } \mathrm{NGI} \tag{3.2}$$

Where NGI refers to *facies* Net-to-Gross Index, VCI is Vertical Connectivity Index, and LCI is Lateral Connectivity Index. Both VCI and LCI are defined as follows:

Vertical Connectivity Index

The Vertical Connectivity Index (VCI) was previously called Sand Connectivity Index (Omoniyi et al., 2013; Omoniyi et al., 2014; Omoniyi et al., 2015). The VCI expresses apparent connectivity in a wellbore or over a vertical interval in an outcrop section. It is a product of NGI and Vertical Connectivity Factor (VCF). That is:

$$\mathrm{VCI} = \mathrm{NGI} \text{ x } \mathrm{VCF} \tag{3.3}$$

NGI is mathematically defined in Equation 3.1 and VCF is calculated as follows:

$$VCF = \left[{}^{S/S} \Big/ \left({}^{S}/_{S} + {}^{S}/_{NS} \right) \right] \quad (3.4)$$

where S/S is the proportion of sand overlying sand, and S/NS represents the ratio of sand overlying non-sand/non-silt lithology.

VCI varies from 0 to 1. Low VCI values imply low apparent vertical connectivity and high VCI values indicate high apparent vertical connectivity.

Lateral Connectivity Index

The Lateral Connectivity Index (LCI) refers to the apparent lateral connectivity of respective TBT/VTBT facies and related sandbodies within the interval being considered. In other words, it is defined as:

$$LCI = \left[{}^{(h_1/X)\ x\ n_1} \Big/ {}_{(h_2/X)\ x\ n_2} \right] \quad (3.5)$$

where h_1 & h_2 are interval thicknesses at two locations (1 and 2);
X is the distance separating the two locations; and
n_1 & n_2 represent number of beds within the interval under consideration at location 1 and location 2, respectively.

LCI varies from 0 to 1. Low LCI values imply low apparent lateral connectivity and high LCI values indicate high apparent lateral connectivity.

3.2.2.3 Facies Ratio Index

The Facies Ratio Index (FRI) is derived from the proportion of TBT beds to the sum of TBT and VTBT beds in a characteristic facies association. It is therefore distinctive of different depositional environments, proximal to distal relationships and/or near-to-far channel location. It compares to Bouma/Stow sequence combination and selected facies ratios. That is:

$$FRI = \left[{}^{nTBT}/_{\sum n(TBT;\, VTBT)} \right] \quad (3.6)$$

nTBT refers to number of TBT beds in a distinctive facies association being considered, and $\sum n(TBT; VTBT)$ is the sum of TBT and VTBT in the facies association. FRI ranges from 0 to 1 and it is indicative of the energy condition prevalent during sediment transport and subsequent deposition.

3.2.2.4 Sediment Textural Index

The Sediment Textural Index (STI) is derived from the mean grain-size property of all the TBT-VTBT facies in the specific facies association being considered. In particular, it is a measure of the difference in mean grain size between the coarser-grained (sandstone-siltstone) beds and the finer-grained (mudstone-rich) interbeds. It therefore takes into account the relative ease with which fluid can migrate through and be stored within the mudstone interbeds compared with the sandstone beds. It can provide insight into sediment transport, depositional history and sediment maturity.

The STI is calculated by taking the reciprocal of mean grain size in phi units ($\bar{\delta}m$) of all the mud-rich interbeds minus the mean grain size in phi units ($\bar{\delta}s$) of all the sand-rich beds in the facies association being considered. In each case, the nearest whole number phi unit is used. This is then multiplied by the NGI in order to account for the relative thickness of sandstone versus mudstone. This therefore becomes:

$$STI = \left({}^{1}/_{(\bar{\delta}m - \bar{\delta}s)} \right) x\ NGI \quad (3.7)$$

STI ranges from 0 to 1, where values closer to 0 represent a large difference between sand and mud mean grain size and relatively thicker mudstone interbeds, whereas values closer to 1 represent a small difference between the sand and mud mean grain size and relatively thinner mudstone interbeds.

3.2.3 Laboratory-based property measurements of TBT/VTBT facies plugs

The variability of reservoir properties of TBT and VTBT is usually difficult to predict, particularly, in the presence of sparse data. Prediction of these properties in hydrocarbon

reservoirs is critical in clastic turbidite reservoirs with a significant proportion of TBT and VTBT facies, and it impacts prospect evaluation, reserve estimation, reservoir development and depletion strategy. Laboratory-based measurements of core plugs provide the most direct way to determine rock mechanical data (Ameen et al., 2009). However, these measurements are mostly replaced with measurements derived from wireline logs because of the high cost of coring wells. The two properties of interest to this research are porosity and permeability. These properties were measured on representative core plugs and, the results were used where there were no cores for laboratory-based measurements (Chapter 6), and to quality-control the measured properties used in Chapters 5 and 7. Laboratory-based porosity measurements were also correlated with wireline log-derived porosity (Chapter 4) in order to establish a porosity trend for uncored intervals.

3.2.3.1 Sample preparation

Forty eight cylindrical core plugs (hereafter referred to as plugs) were acquired from a North Brae Field well, 16/07a-B27, using Eibenstock EBM 250\2P coring machine with 25.25 mm (~1.0 in) diameter drill (Figure 3.4). Coring was carried out at discrete points to include the six TBT/VTBT facies associations identified in the North Brae Field. The resultant plugs were accurately trimmed, at both ends, to desired dimensions, using a Cutrock GSP 1463 trimming saw (Figure 3.5). Water supplied from a tap was used as a lubricant during coring and trimming of plugs. The trimmed plugs (Figure 3.6) were appropriately labelled using a permanent marker, and kept on a flat surface within the laboratory, to dry for six days.

3.2.3.2 Principle and procedure for porosity measurement

On the seventh day, a digital vernier caliper was used to measure plugs' dimensions (i.e. diameter and length). For each measurement, three readings were taken and the average value was calculated and recorded. This average value enhanced precision of dimensions measured. Each plug was then placed in the specimen chamber of a helium gas expansion Porosimeter MK II (Figure 3.7, A). The porosimeter has an output channel, which provides an opportunity for interfacing with a computer for calibration, data storage and analysis. This equipment is capable of porosity measurements over a range of different

Figure 3.4. A photograph showing an Eibenstock EBM 250\2P coring machine, being safely operated at Geomechanics Workshop (HWU, Edinburgh). The machine was powered by electricity, and coring core slab was done by gently lowering the drill using the drill control. Water was supplied through a hose connected to a tap, and served as a lubricant to ease coring.

Figure 3.5. A photograph showing a Cutrock GSP 1463 trimming saw, being safely operated at Geomechanics Workshop (HWU, Edinburgh). The machine was powered by electricity, and trimming of plugs was done by carefully turning the ‘control wheels’. Water was supplied through a hose connected to a tap, and served as a lubricant to ease trimming.

Photo was taken by Bayonle Omoniyi

Figure 3.6. A photograph showing selected plugs cored from 16/07a-B27, North Brae Field.

plug sizes without modification and can be easily calibrated. It operates on the principle of Boyle's Law (Figure 3.7, B). This law states that, for an ideal gas, at constant temperature, the multiple of its pressure and volume is a constant (Equation 3.8).

$$P_1V_1 = P_2V_2 \tag{3.8}$$

The gas transfer technique involves the injection of helium gas into the space with known volume. It is then allowed to expand into another space also with known volume. By placing a plug of unknown grain volume in the second space and measuring the final pressure of the helium in the space, the unknown grain volume (V_f) of the sample can be calculated using Equation 3.9:

$$V_g = \left[118.12 - \left({}^{1720.32}/_{P}\right)\right] - V_f \tag{3.9}$$

where P is pressure (in Pascal) of the plug being measured and, V_f is the filler volume (cubic centimetre). The filler volume is the known (cylinder) volume where the filler is used. Where no filler is used, filler volume is zero. The pressure, P, is read out from the helium regulator meter (see the dotted red arrow in Figure 3.7, A).

For each plug placed in the specimen chamber (see the thick red arrow in Figure 3.7, A), its grain volume was calculated by the difference in final pressure between the initial pressure (when the chamber is empty) and final pressure (with the plug in the chamber). When the key is open to allow gas supply, it (helium gas) penetrates all the pore spaces that are available for flow. Consequently, the volume taken up by the plug in the chamber is that, which is occupied by the grains and the pores that are not connected with the plug surface. Thus, the porosity calculated through this method is the effective porosity (not total porosity). According to Stocks (2009), effective porosity is a measure of pores that are in communication such that fluids can pass through the pore system.
For measurement of the forty-eight plugs, the gas supplied was allowed to settle in the core chamber, so the first pressure reading was not recorded. Subsequently, three pressure readings were taken and their average was recorded to ensure precision.

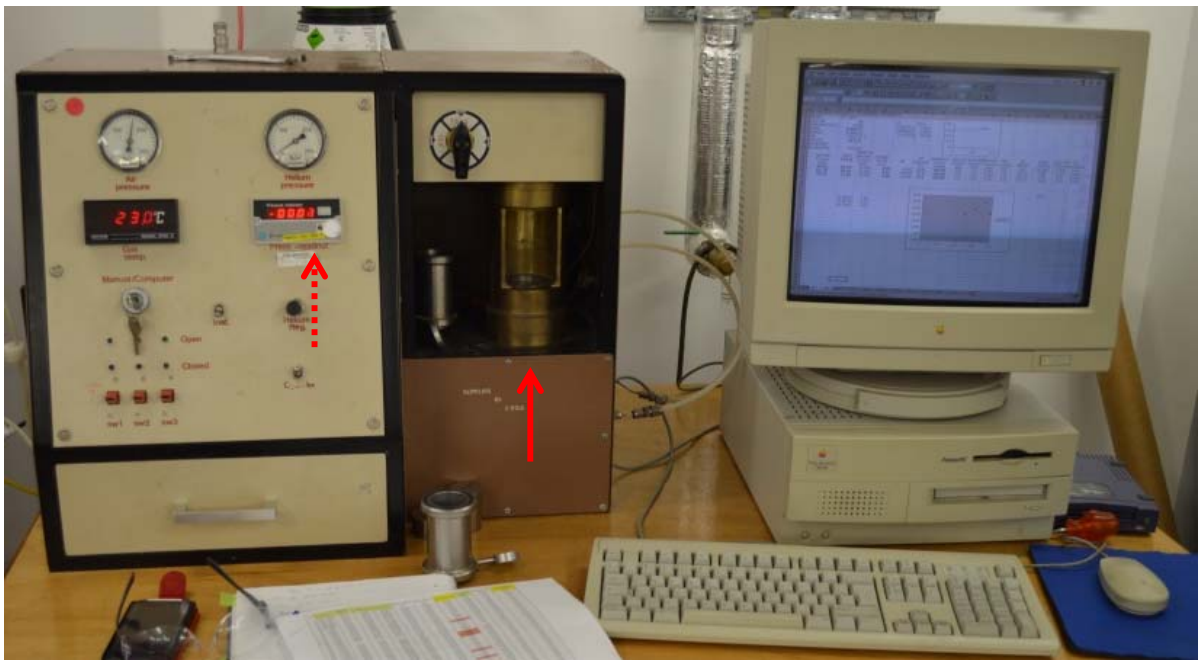

A.

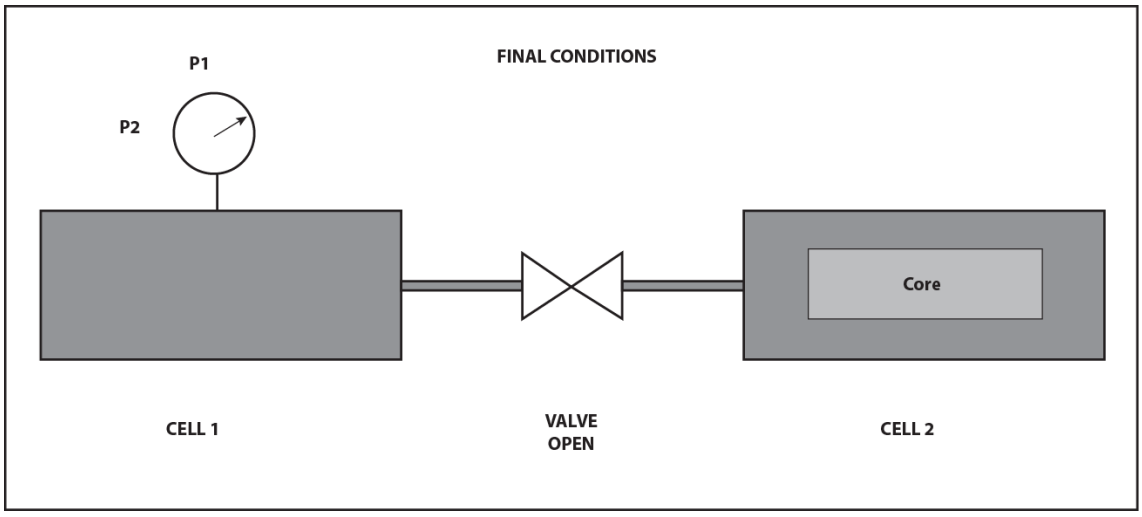

B.

Figure 3.7. (A) A photograph showing a Helium gas expansion Porosimeter MK II that was used to measure porosity of representative TBT/VTBT plugs. The red arrow points to core chamber and dotted arrow marks helium regulator meter from which the pressure value is read. (B) A sketch showing the operating principle upon which the porosity measurement is based.

3.2.3.3 Principle and procedure for permeability measurement

The permeability of the plugs was measured using EPS Nitrogen Gas Permeameter. This equipment was designed to eliminate potential sources of error and inaccuracy. It was connected to two nitrogen supplies to obtain desired confining pressure (300 pounds per square inch, psi) using a 0-100 psi regulator (Figure 3.5). All permeability measurements were made under a backpressure flow mode to provide accurate control of core pressure and flow rate, and to maintain laminar flow rates, particularly in high-permeability plugs. This mode is preferred to flow under atmospheric pressure (i.e. forward flow) because it restricts the development of non-Darcy flow, over a variety of flow/pressure conditions. However, for this mode (backpressure flow), a transducer zero shift correction was carried out. The zero shift is a phenomenon that is caused by unequal stresses acting on the diaphragm of the transducer when a pressure, greater than the ambient calibration pressure, is applied equally to both sides of the diaphragm (EPDS User manual). The differential and gauge transducers of the instrument were calibrated by a Geomechanics specialist (Sally Hamilton).

The permeability of each of the forty-eight plugs was measured by gently placing it in the core sleeve so that it lies horizontal and fits easily into the sleeve and allows adequate clearance for loading. Care was taken to ensure that the plug was centrally located within the coreholder (red arrow in Figure 3.8). The fluid distributors were located against the plug face and locked in position by evenly hand-tightening the two locknuts, located at both ends of the core sleeve. Approximately the same amount of thread must be evident on each locknut to prevent gas leakage. Care was also taken to ensure that fluid distributors did not move within the core sleeve. The procedure for operating the instrument (Figure 3.9) was then carefully followed.

The operational principle is based on the fact that a gas is compressible, whereas a liquid is incompressible. Thus, the pressure of nitrogen gas decreases, causing the gas to expand as it flows towards the downstream end of the sample in the coreholder. This phenomenon forms the basis for formulating an expression for calculating core permeability to nitrogen gas, k_n, under laminar flow conditions. This is expressed as:

$$k_n = \left(\mu \times Q_b \times P_b \times L\right) \Big/ \left(A \times \Delta P \times P_m\right) \tag{3.10}$$

where μ is gas viscosity (centipoise) and was obtained from Equation 3.11:

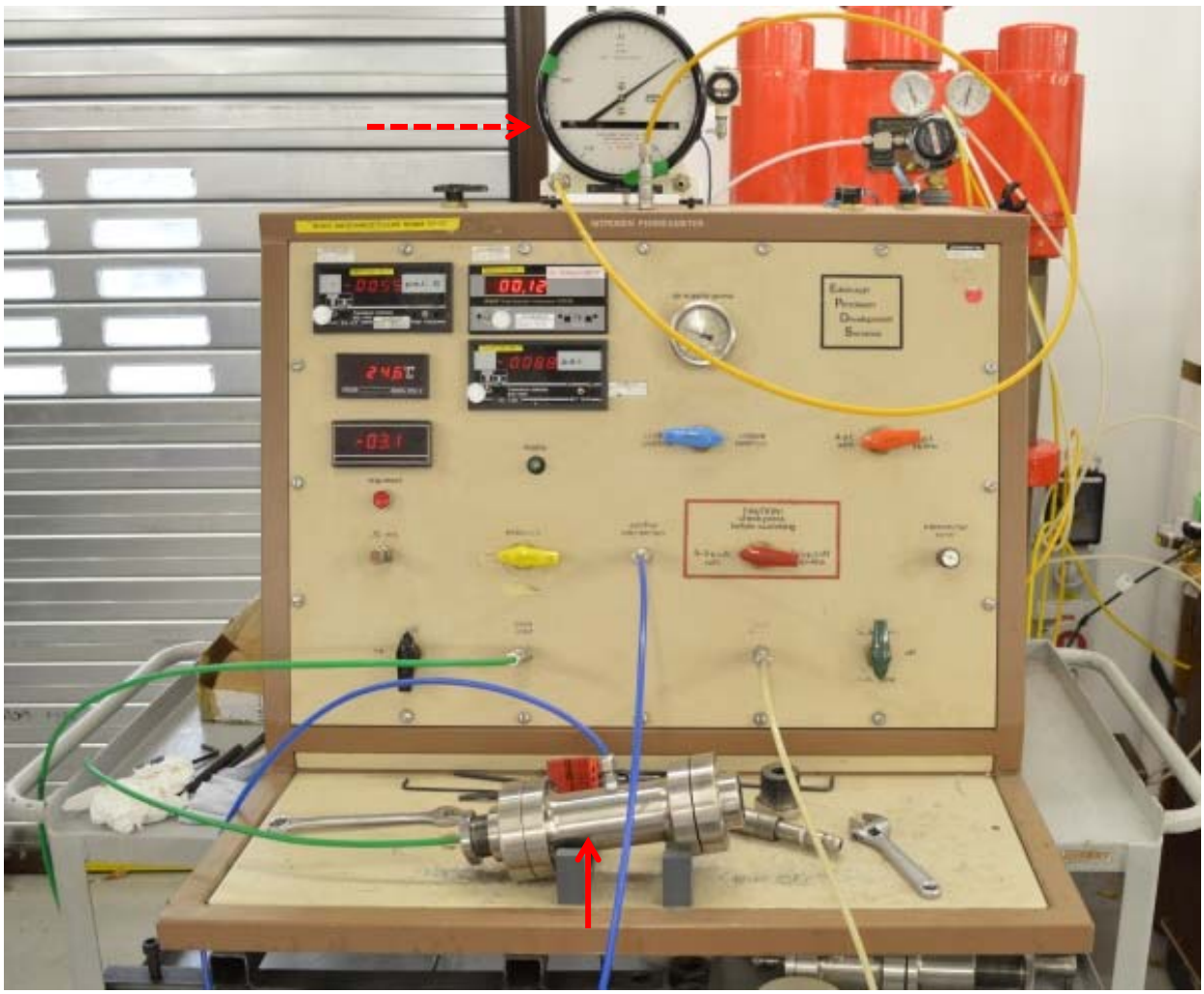

Photo was taken by Bayonle Omoniyi

Figure 3.8. A photograph of EPS Nitrogen Gas Permeameter. The thick red arrow indicates the coreholder, whilst the dotted red arrow points to the flow meter.

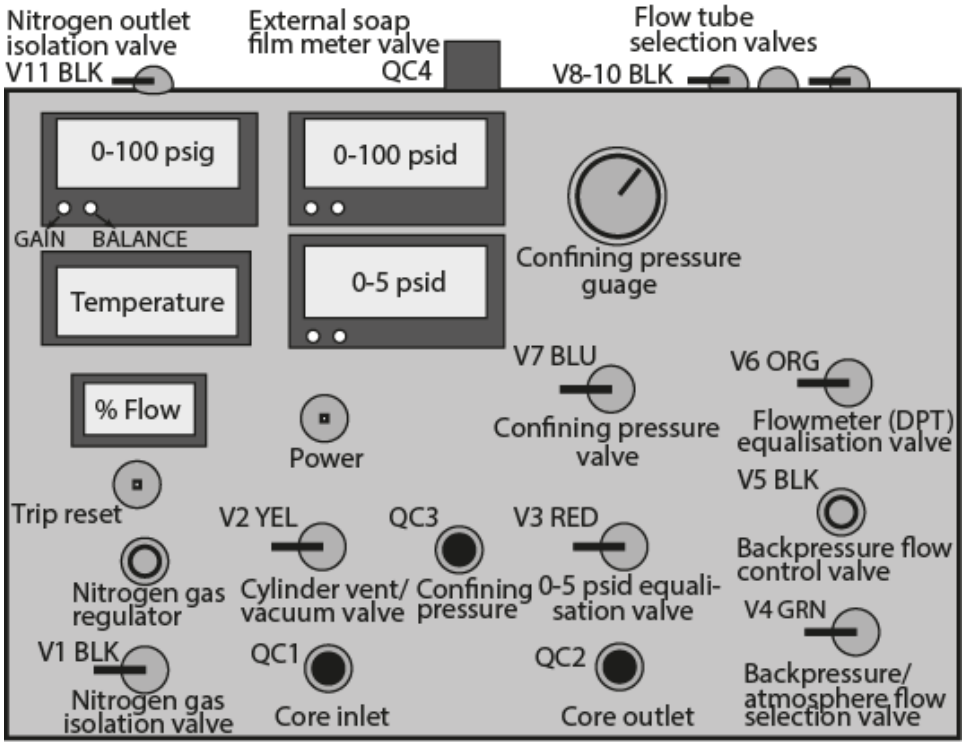

Procedure for backpressure flow operation of an EPS Nitrogen Permeameter

1. Record temperature. This should be constant throughout the measurement if the laboratory conditions are not changed.
2. Record atmospheric pressure on barometer. This is also unlikely to change throughout the measurement.
3. Ensure that the regulators (if two nitrogen supplies will be used) are turned to attain required pressure.
4. Turn Valve V4 to BACKPRESSURE.
5. Keep Valve V5 closed, and Valves V3A and V3B in SAFE positions
6. Select desired flow tube capacity, using Valves V8, V9 or V10.
7. Turn Valve V6 to “IN LINE”.
8. Gradually increase nitrogen pressure using regulator valve until desired upstream pressure is set on the 0-100 psig transducer display.
9. Slowly open Valve V5 until desired percentage flow rate is registered.
10. Once stable pressure is achieved, note upstream pressure (0-100 psig), differential pressure (0-100 psid), and gas flow rate.
11. To obtain another reading, if required, close Valve V5 before increasing pressure. Then, open Valve V5 until the desired pressure flow conditions are obtained.
12. When the final pressure reading has been recorded, back off regulator valve completely and slowly open Valve V5 to maintain an atmospheric flow rate of less than 100%, until the plug is completely depressurised.
13. Release confining pressure by turning Valve V7 to “RELEASE” position. Unload the plug from the coreholder.

Figure 3.9. An operational sketch of EPS Nitrogen Permeameter with procedure for backpressure flow operation.

$$\mu = (0.00005 \text{ x } T_m) + 0.0164 \quad (3.11)$$

T_m is gas temperature during test (°C)

Q_b is atmospheric gas flow rate (cc/s) at base or atmospheric pressure P_b (atmospheres). For this study, Q_b was obtained from measurements of actual flow rate, read from a wet gas meter, and calculated from Equation 3.12:

$$Q_b = {}^{\text{revolution (cc)}}\!/_{\text{time (s)}} \quad (3.12)$$

where P_b is ambient pressure (atmospheres). This pressure was obtained by measuring atmospheric pressure on a mercury barometer (P_t) and substituting the value into Equation 3.13:

$$P_b(\text{atm}) = {}^{P_t \text{ (mm Hg)}}\!/_{760} \quad (3.13)$$

From Equation 3.10, L and A are the plug's length and area, respectively. The area was calculated using the plug dimensions. ΔP is differential pressure (atmospheres), obtained as the difference between plug upstream pressure (P_1) and downstream pressure (P_2). That is:

$$\Delta P = P_1 - P_2 \text{ (atmospheres)} \quad (3.14)$$

Since backpressure method was used, then

$$P_1 = \left[\frac{P_1(\text{psig})}{14.7} + P_b(\text{atmospheres})\right] \quad (3.15)$$

$$P_2 = \left[\frac{P_1(\text{psig})}{14.7} - \frac{\Delta P \text{ (psid)}}{14.7}\right] + P_b(\text{atmospheres}) \quad (3.16)$$

Both P_1 and ΔP were obtained directly from the '0-100 psig' and '0-100 psid' readouts (see Figure 3.9 and step 10 in the procedure), and P_m is the plug mean pressure that was calculated, using Equation 3.17:

$$P_m(\text{atmospheres}) = \left[{(P_1 + P_2)}/{2}\right] \quad (3.17)$$

where P_1 and P_2 are upstream and downstream pressures, respectively.

The Klinkenberg permeability is based on the Klinkenberg principle: gas permeability decreases as the mean gas pressure in core increases. By plotting gas permeabilities obtained at different mean core pressure against reciprocal mean pressure (Figure 3.10), the intersection point on the gas permeability axis, when the resulting straight line is extrapolated to infinite mean pressure, corresponds to the "liquid" permeability. The permeability value at that point is the Klinkenberg permeability for the plug, and is related to Equation 3.18.

$$k_L = \left[\frac{k_n}{\left(1+{b}/{P_m}\right)}\right] \quad (3.18)$$

where k_L is theoretical liquid permeability, k_n is permeability to nitrogen gas, and b is Klinkenberg factor. This factor is inversely proportional to liquid (oil) permeability, (k_L), and corresponds to the slope of the straight line (see Figure 3.10).

After measurement of a plug was completed, the plug was unloaded from the coreholder by fully venting core line pressure and confining pressure directly to the atmosphere, via a selected flow tube. The two locknuts were loosened. One locknut and distributor were removed from the coreholder, and the plug was pushed out, using the other distributor. After unloading the plug, another plug was loaded and the procedure in Figure 3.9 was repeated. The procedure was followed for all the plugs that were successfully measured. The key uncertainties associated with porosity and permeability measurements of the plugs are listed in Table 3.1.

3.2.4 Reservoir modelling

Reservoir models are capable of reflecting the complex nature of hydrocarbon reservoirs over a range of scales that can capture the degree of heterogeneity within such reservoirs (Cosentino, 2001; Caers, 2005; Bentley & Smith, 2008; Ringrose & Bentley, 2015). For this research, Petrel 2015 package was used to build scenario-based reservoir models

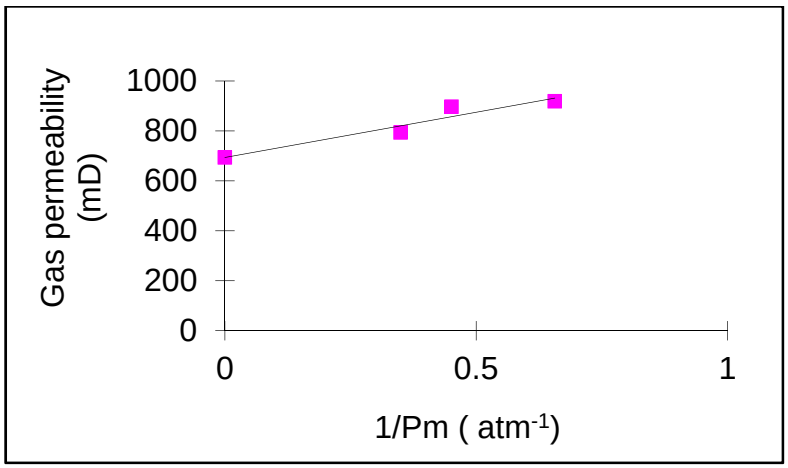

Figure 3.10. Schematic plot of gas permeabilities at mean core pressure versus reciprocal mean pressure for a plug. The three readings read for this plug are plotted, and the intersection point on the gas permeability axis corresponds to the Klinkenberg permeability for the plug.

Table 3.1. Uncertainties associated with core-based porosity and permeability measurements.

Uncertainty	Source	Impacts	*Rank	Mitigation
Dimensions: length, diameter	Unevenly trimmed samples	Bulk volume, which in turn impacts pore volume	5	Three readings for each plug were taken and their average recorded
Weight	Water used for coring and trimming	Water may increase sample weight. This impacts bulk and grain densities	4	Samples were thoroughly dried before weighed. Three weight readings were taken and their average recorded
Temperature	Calibration of Permeameter	Bulk and pore volume	5	Measurements were done under the same temperature as the prevailing calibration temperature
Nature of fluid	Klinkenberg permeability assumes the presence of an inert non-reactive liquid	Variable permeability caused by the presence of a wetting fluid	3	Samples were dried to get rid of fluids
Deviation from laminar flow, particularly in high permeability samples	Poorly regulated gas supply	Lack of control on flow rate and pressure, causing erroneous Klinkenberg permeability	2	Selection of backpressure flow mode to gain control on flow rate. Appropriate regulator was used for gas control

*Ranks (1-5) based on their impact, 5 highest impact, 1 lowest

primarily to estimate oil recovery, evaluate reservoir flow performance in TBT/VTBT facies and associated deepwater architectural elements, assess the impact of connectivity at a scale of inter-well spacing, and assess the range of uncertainty associated with the flow performance. In building these reservoir models, core and wireline log data were used to develop stratigraphic schemes. These schemes formed the basis for the various scenarios considered in the respective studies (Chapters 5 and 7). Petrophysical data, comprising porosity and permeability, were sourced from core-based porosity and permeability data from selected wells in the North Brae Field. Net-to-gross property for the wells used were generated from volume of shale (Vsh) models that were derived from gamma ray logs and neutron-density logs, using Techlog 2014 package.

The three-dimensional (3D) reservoir models built and presented in this thesis reflect the various degree of heterogeneity, varying from geological layers captured in the models, lithological spatial distribution and lateral variation, to variation in net-to-gross, porosity and permeability. The scale of heterogeneity considered sufficient to achieve the research objectives, informed the model resolution chosen in respective studies in this thesis (Chapters 5-7). Full-field reservoir models were not considered, thus, by focussing on small sector, it was possible to build high-resolution grids without an extremely large number of grid cells. Because of pitfalls inherent in grid upscaling (Figure 3.11), and the scale of heterogeneity considered adequate to achieve the research objectives, the 3D grids were built at high resolution, and they were found to be geologically consistent to allow flow simulation without upscaling. These high-resolution models reveal the heterogeneity in the spatial distribution of reservoir net-to-gross, porosity, and permeability within the segments considered in subsequent chapters.

The term 'facies' used to describe 3D models in Chapters 5 and 7 refers to facies associations 1-4 (i.e. $FA1_{NBF}$-$FA4_{NBF}$). The facies population was distributed within the 3D grids, using Sequential Indicator Simulation (SIS) approach (Chapters 5 and 6) and object-based approach (Chapter 7). Geometrical parameters estimated from wireline-log correlation informed the anisotropy range and orientation of the constituent facies associations in the facies models. The well tops were matched with the top of the Brae Formation as datum. In the absence of interpreted seismic volume and resultant facies probabilities, facies types and proportion in the 3D object-based models were constrained, using estimation made from wireline log and core data. The property modelling approach used in the respective modelling sections, is Sequential Gaussian Simulation (SGS). This approach honours well data, input proportions and distributions, and the property variograms for the property data being modelled. Generally, populating the 3D grids with

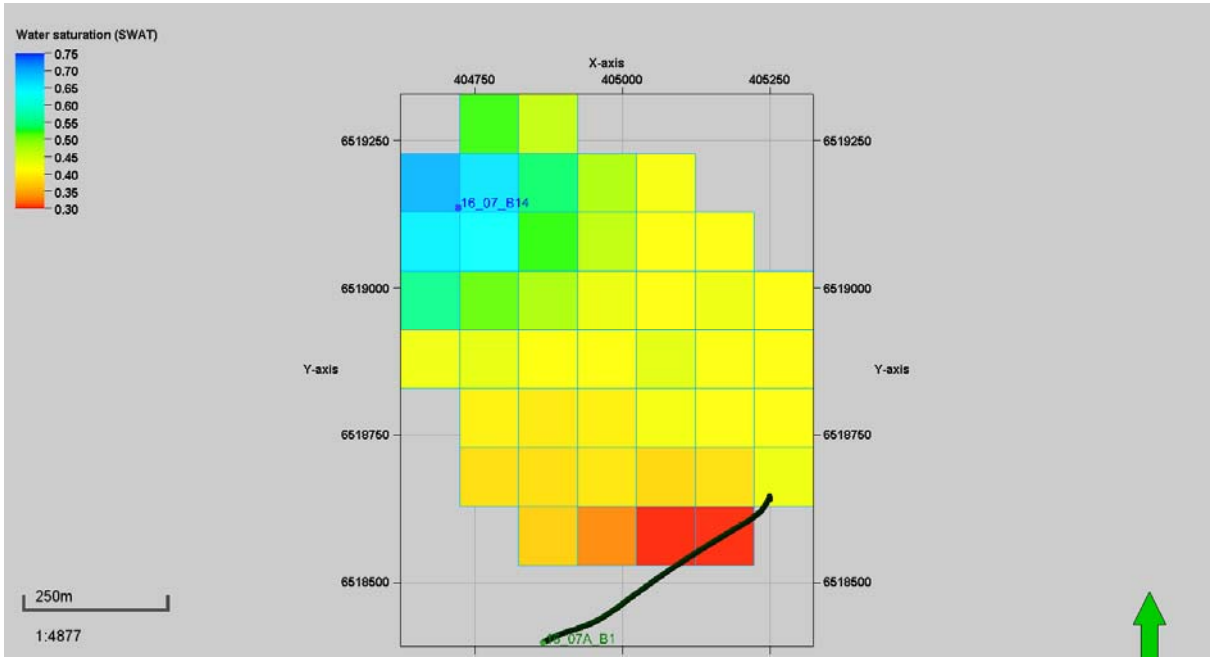

A.

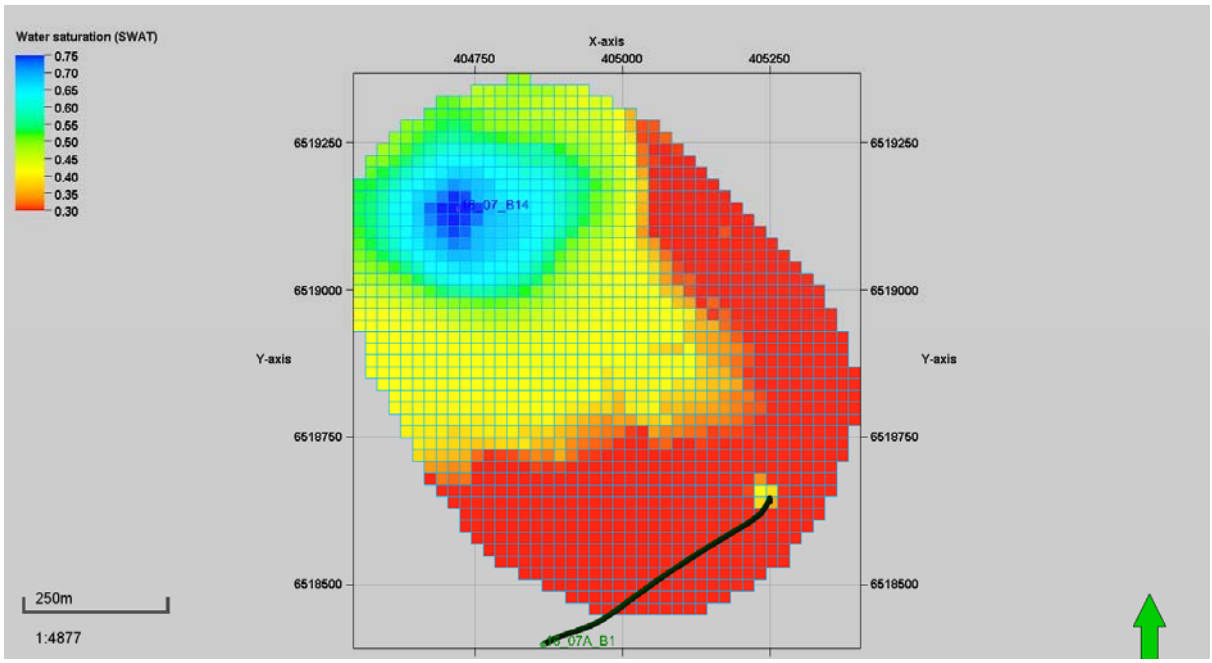

B.

Figure 3.11. Effect of coarse grid in a layered reservoir model. (A) Low resolution (or coarse-scale) grid, with grid size of 100 ft x 100 ft. In this grid, water saturation pattern cannot be used to decipher the heterogeneity in the system. (B) High-resolution (fine-scale) grid, with grid size of 20 ft x 20 ft. In this grid, the scale of heterogeneity in the system is obvious as reflected in the water saturation profile for the same date in A (above). The downside to high-resolution grids is the large amount of time it takes to perform property modelling and flow simulation. This is however compensated for by the amount of heterogeneity the grid is able to capture. High resolution grids were used throughout the simulation studies in this thesis.

the reservoir property was based on the facies-influenced distribution of the property. In other words, if a grid cell consists of $FA1_{NBF}$, the value of the property being modelled for $FA1_{NBF}$ will be assigned to the cell. This assignment is automatically executed by the modelling algorithm (SGS) for all the cells in the grid.

3.2.5 Reservoir flow simulation

For the reservoir flow simulation studies, water injection was used to aid water drive (otherwise referred to as aquifer drive). Where the displacement process is not fully supported by water drive, a secondary recovery mechanism such as gas or water injection, could support reservoir pressure, by maintaining reservoir energy and displacing oil (Cosentino, 2001; Carlson, 2006; Fanchi, 2006; Sorbie et al., 2013). For modelling immiscible two-phase (oil and water) flow process in the porous media considered in this research, a black-oil simulator (Petrel 2015 package) is preferred to the others (compositional, miscible, thermal and chemical) because it provides the best approach, and does not model the full effects of composition in the two phases (note that modelling compositional effects is outside the scope of this research). For all the simulation cases considered, a simple saturation function model was adopted (Figure 3.12). This saturation function model was considered adequate to achieve the objectives of the flow simulation studies.

The reservoir flow simulation studies in this thesis are based on the principle of Darcy's Law. The law stems from a series of flow tests in sand filters (for drinking water in Lyons, France), conducted in 1856, by Henri Darcy (a French civil engineer). Darcy's Law provides the understanding of fluid flow through a porous media, and it is represented by Equation 3.19.

$$Q = -A\frac{k}{\mu}\frac{\partial \Phi}{\partial x} \tag{3.19}$$

where Q is flow rate (cm^3/s), A is cross-sectional area of flow (cm^2), ∂x is length of the sand pack, $\partial \Phi$ is applied pressure drop, k is permeability (darcy), and μ is viscosity (centipoise) (Carlson, 2006).

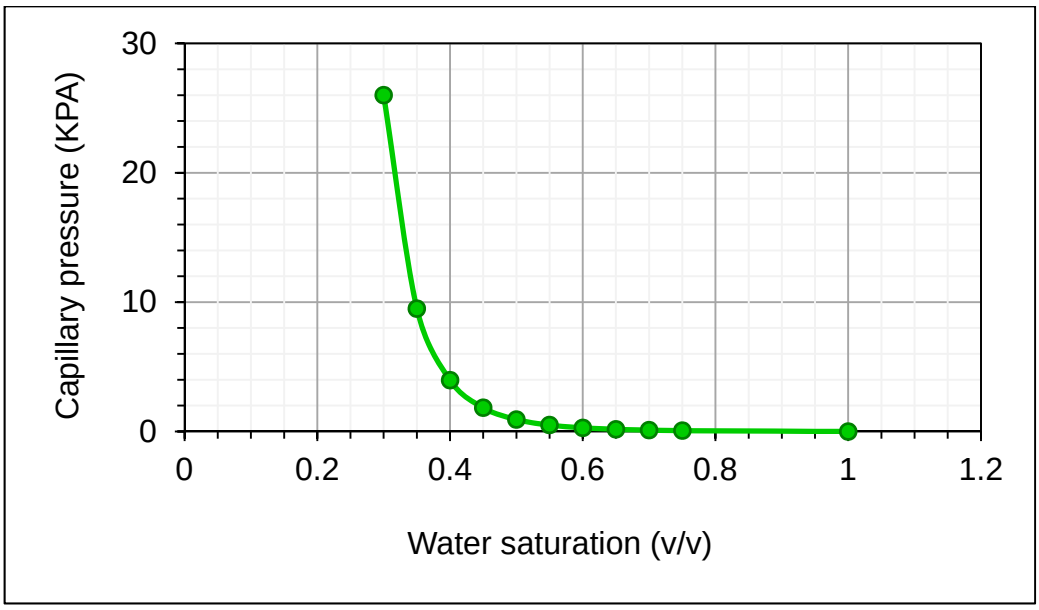

Figure 3.12. Schematic saturation function model used for reservoir flow simulation.

Equation 3.19 has since been transformed into a single-phase Darcy's Law. That is:

$$Q = -\beta \frac{kA}{\mu}\left[\frac{\Delta P}{L}\right] \tag{3.20}$$

where Q is flow rate (cm^3/s), β is conversion factor (dimensionless), usually 1.00, k is permeability of the porous media (darcy), A is cross-sectional area of flow (cm^2), μ is viscosity (centipoise), ΔP is pressure drop (atmosphere), and L is length of the system (cm). The complete definition of these parameters are provided in Table 3.2.

It is important to note that during the waterflood simulations performed for the various studies in this research, the single-phase (oil) Darcy's Law applies, in as much as only oil is flowing into the producer well. Following water breakthrough (when water reaches the producer well), both oil and water are produced from the producer well. Consequently, the single-phase Darcy's Law no longer holds, but it is replaced with the immiscible two-phase (oil and water) Darcy's Law for each of the two phases (Equations 3.21 and 3.22).

$$Q_o = \frac{k.k_{ro}A}{\mu_o}\left(\frac{\Delta P_o}{L}\right) \tag{3.21}$$

$$Q_w = \frac{k.k_{rw}A}{\mu_w}\left(\frac{\Delta P_w}{L}\right) \tag{3.22}$$

where Q_o and Q_w are flow rates of oil and water, respectively;
k is absolute permeability;
k_{ro} and k_{rw} are the relative permeabilities for oil and water, respectively;
A is cross-sectional area of the system;
μ_o and μ_w are the oil and water viscosities, respectively;
ΔP_o and ΔP_w are the pressure drops across the oil and water phases, respectively; and
L is length of the system.

The black-oil simulator used for the reservoir flow simulation studies is capable of generating the flow rates for both single-phase and two-phase Darcy's Laws and present the output in a format that can be easily exported to any output processing platform. For this purpose, Matlab (R2017a) skills became handy. Prior to performing simulation, the following were carefully considered:

Table 3.2. Definition of parameters in the single phase Darcy's Law (modified from Sorbie et al., 2013).

Definition	Symbol	Dimensions	Units			
			Centimetre-gram-second (cgs)	Laboratory	Field	International System (SI)-Field
Flow rate	Q	L^3/T	cm^3/s	cm^3/s	bbl/d	m^3/d
Length of system	L	L	cm	cm	Ft.	m
Cross-sectional area	A	L^2	cm^2	cm^2	$Ft.^2$	m^2
Viscosity	μ	nil	cP	cP	cP	Pa.s
Pressure drop	ΔP	$M.L.T^2$	atm	$dyne/cm^2$	psi	Pa
Permeability	k	L^2	darcy	Darcy	mD	mD
Conversion factor	β	dimensionless	1.00	$9.869x10^{-6}$	$1.127x10^{-3}$	$8.527x10^{-3}$

*bbl/d = barrel per day; Pa.s=Pascal second; atm=atmosphere; psi=pounds per square inch; cP=centipoise; mD=milliDarcies

i. Model grid dimensions. The reservoir model grids were built at high resolution adequate to capture the scale of heterogeneity being considered, without having to coarsen the grids. Grid upscaling is capable of blurring or removing geological details (Figure 3.11), which may improve the simulation.

ii. Grid properties. The grid properties were fed by the petrophysical properties, after quality-control measures such as normalisation, and removal of spike and trend in petrophysical properties were carried out. The refined petrophysical properties were upscaled using arithmetic average, and subsequently, conditioned to facies distribution (see the ensuing chapters).

iii. Fluid properties. Default fluid properties for black oil model (Petrel 2015 package) were adopted for all the simulations performed.

iv. Initial conditions. Reservoir pressure, datum depth (e.g. Top Brae Formation), oil-water contact (or free water level) form the primary initial conditions required for set up in a simulation study. Default settings were used for the J-Function parameters.

v. Output format. The simulation results comprise flow properties of interest that give an indication of reservoir flow performance in the scenarios considered for the respective simulation studies. These properties include oil production rate, rate decline, oil recovery efficiency, water cut, cumulative oil production, and oil displacement pattern.

vi. Production schedule. Different production schedules were used for the flow simulation studies. Details of the production schedule are presented in the related chapters in this thesis.

The well flow rates considered for the studies (20,000 bbl/d in Chapters 5 and 7, and $50\ \mathrm{sm}^3/\mathrm{d}$ in Chapter 6) were calculated using Equation 3.23 for a single phase Darcy's Law.

$$Q = PI(P_e - P_{wf}) \tag{3.23}$$

where Q is flow rate, PI is productivity index, P_e is reservoir pressure, and P_{wf} is well flowing pressure.

The highest flow rate can only be achieved when $P_{wf} = 0$. That is:

$$Q = PI(P_e - 0) \tag{3.24}$$

$$Q = PI.P_e \tag{3.25}$$

The productivity index (PI) is calculated from Equation 3.26.

$$PI = \frac{2\pi(k.h)}{\mu.In\left[{r_e}/{r_w}\right]} \tag{3.26}$$

where k is absolute permeability, h is reservoir thickness, μ is viscosity, r_e is the effective radius of the reservoir, and r_w is the radius of the wellbore. Note that r_e is also the drainage radius and is calculated from a complex equation (Equation 3.27) that holds for anisotropic permeabilities.

$$r_e = 0.28\ \frac{\left[\left(\frac{k_y}{k_x}\right)^{1/2}.x^2+\left(\frac{k_x}{k_y}\right)^{1/2}.y^2\right]^{1/2}}{\left(\frac{k_y}{k_x}\right)^{1/4}+\left(\frac{k_x}{k_y}\right)^{1/4}} \tag{3.27}$$

Equations 3.23-3.27 (modified from Carlson, 2006; Sorbie et al., 2013) are automatically calculated by the black oil simulator, and the results generated as output data for further processing.

3.2.6 Uncertainty

In this research, uncertainty analysis focuses on selected parameters that are aligned to the research objectives. For this purpose, the analysis focuses on attribute indices (NGI and SCI), oil recovery and reservoir flow performance. The analysis is limited to assessment, using probability density function (pdf) and cumulative distribution function (cdf), whilst its quantification, related to Baye's Rule, is outside the scope of this research.

3.2.7 Basic statistics

The basic statistics applied in this thesis are range, arithmetic mean, and standard deviation. These measures of dispersion are defined as follows:

i. Range: This is the difference between the highest and lowest values of a sample population. That is:

$$\text{Range} = \text{highest value} - \text{lowest value} \tag{3.28}$$

ii. Arithmetic mean: This is obtained by adding all the values of all individual samples and then dividing the sum by the size of the population. That is:

$$\mu = {(x_1 + x_2 + x_3 + \cdots + x_n)}/{N} \tag{3.29}$$

Alternatively,

$$\mu = {1}/{N} \sum_{i=1}^{N} x_i \tag{3.30}$$

where variables $x_1, x_2, x_3, \ldots, x_n$ are sample values, N is the size of the population (i.e., number of individuals in the population), and i represents individual sample number (1, 2, 3,…x_n).

iii. Standard deviation: Standard deviation is a measure that is used to quantify the amount of dispersion of a set of data values. It is calculated using Equation 3.31.

$$s = \sqrt{{\sum (x - \bar{x})^2}/{n - 1}} \tag{3.31}$$

where x is an individual sample value, $\bar{x}$ is the sample mean, and n is the sample size.